

## Supplementary Information for:

Characterization of the earliest intermediate of Fe-N<sub>2</sub> protonation: CW and Pulse EPR detection of an Fe-NNH species and its evolution to Fe-NNH<sub>2</sub><sup>+</sup>

Mark A. Nesbit, Paul H. Oyala\*, Jonas C. Peters\*

Division of Chemistry and Chemical Engineering, California Institute of Technology (Caltech),  
Pasadena, California 91125, United States

### Contents

<b>Experimental and Synthetic Details</b>	<b>S2-S15</b>
<b>Crystallographic Information</b>	<b>S16</b>
<b>Additional HYSCORE Data and Simulations</b>	<b>S17-S24</b>
<b>Comparison of ESE-EPR of Isotopologues of <sup>Ar</sup>P<sub>3</sub><sup>B</sup>Fe(NNH)</b>	<b>S25</b>
<b>Additional ENDOR Data</b>	<b>S26-S27</b>
<b>CW EPR Spectrum of <sup>Ar</sup>P<sub>3</sub><sup>B</sup>Fe(NNSiMe<sub>3</sub>) with Simulation</b>	<b>S28</b>
<b>Orientation of <sup>1</sup>H Hyperfine Tensor in [<sup>Ar</sup>P<sub>3</sub><sup>B</sup>Fe(NNH<sub>2</sub>)]<sup>+</sup></b>	<b>S29</b>
<b>NH<sub>3</sub> Production Assay Results</b>	<b>S29</b>
<b>DFT Optimized Structures and EPR Parameters</b>	<b>S30-S35</b>
<b>Electrochemical Data</b>	<b>S36</b>
<b>References</b>	<b>S36</b>

**General Considerations:** All operations were carried out using standard Schlenk or glovebox techniques under inert atmospheres of N<sub>2</sub> or argon. Unless otherwise noted all solvents were deoxygenated and dried by thoroughly sparging with N<sub>2</sub> gas followed by passage through an activated alumina column in the solvent purification system by SG Water, USA LLC and stored over 3 Å molecular sieves prior to use. Non-halogenated solvents were tested with a standard purple solution of sodium benzophenone ketyl in tetrahydrofuran in order to confirm effective oxygen and moisture removal. All reagents were purchased from commercial vendors and used without further purification unless otherwise stated. 4-bromo-2,6-diisopropylanisole, 2-bromophenylphosphorusdichloride, [Na][BAr<sup>F</sup><sub>24</sub>], [H(OEt<sub>2</sub>)<sub>2</sub>][BAr<sup>F</sup><sub>24</sub>] (HBAr<sup>F</sup><sub>24</sub>), KC<sub>8</sub>, Cp\*<sub>2</sub>Co, and [Ph<sub>2</sub>NH<sub>2</sub>][OTf] were synthesized following literature procedures.<sup>1,2,3,4,5,6</sup> Deuterated solvents were purchased from Cambridge Isotope Laboratories, Inc., degassed and stored over activated 3 Å molecular sieves prior to use. Elemental analyses were performed by California Institute of Technology's Elemental Analysis facility or by Midwest Microlab, LLC, Indianapolis, IN.

**Nuclear Magnetic Resonance Spectroscopy:** <sup>1</sup>H and <sup>13</sup>C chemical shifts are reported in ppm relative to tetramethylsilane, using residual solvent resonances as internal standards. <sup>31</sup>P chemical shifts are reported in ppm and referenced externally to 85% aqueous H<sub>3</sub>PO<sub>4</sub> at 0 ppm. <sup>19</sup>F chemical shifts are reported in ppm and referenced externally to trifluorotoluene at -63.72 ppm. <sup>11</sup>B chemical shifts are reported in ppm and referenced externally to BF<sub>3</sub>•Et<sub>2</sub>O at 0 ppm. Solution phase magnetic measurements were performed by the method of Evans.

**Infrared Spectroscopy:** Solid and thin film IR measurements were obtained on a Bruker Alpha spectrometer equipped with a diamond ATR probe.

**EPR Spectroscopy:** Continuous wave X-band EPR spectra were obtained on a Bruker EMX spectrometer on 2-9 mM solutions prepared as frozen glasses in 2-MeTHF. Pulse EPR spectroscopy: All pulse X- and Q-band (9.4-9.7 and 34 GHz, respectively) EPR, electron nuclear double resonance (ENDOR), and hyperfine sublevel correlation spectroscopy (HYSCORE) experiments were acquired using a Bruker ELEXSYS E580 pulse EPR spectrometer. All Q-band experiments were performed using a Bruker D2 pulse ENDOR resonator. X-band ENDOR experiments were performed using a Bruker MD-4 X-band ENDOR resonator, and X-band HYSCORE experiments were performed using a Bruker MS-5 resonator. Temperature control was achieved using an ER 4118HV-CF5-L Flexline Cryogen-Free VT cryostat manufactured by ColdEdge equipped with an Oxford Instruments Mercury ITC temperature controller.

Pulse electron spin-echo detected EPR (ESE-EPR) field-swept spectra were acquired using the 2-pulse “Hahn-echo” sequence ( $\pi/2 - \tau - \pi - \text{echo}$ ).

Pulse ENDOR spectra were acquired using the Davies pulse sequence ( $\pi - T_{RF} - \pi_{RF} - t_{RF} - \pi/2 - \tau - \pi - \text{echo}$ ), where  $t_{RF}$  is the delay between mw pulses and RF pulses,  $\pi_{RF}$  is the length of the RF pulse and the RF frequency is randomly sampled during each pulse sequence. For all ENDOR scans the same  $t_{RF}$  of 1  $\mu\text{s}$  was used, all other acquisition parameters are detailed in the caption for each ENDOR figure. For Q-band  $^{11}\text{B}$  ENDOR experiments in the range from 0-30 MHz, an LP-2500 low-pass filter (Vectronics, Starkville, MS) with a cutoff frequency of 35 MHz was attached in-line with the RF amplifier and ENDOR coils in order to eliminate contributions from  $^1\text{H}$  harmonics in the RF region of interest.

X-band and Q-band Pulse HYSCORE spectra were acquired using the 4-pulse sequence ( $\pi/2 - \tau - \pi/2 - t_1 - \pi - t_2 - \pi/2 - \text{echo}$ ), where  $\tau$  is a fixed delay, while  $t_1$  and  $t_2$  are independently incremented by  $\Delta t_1$  and  $\Delta t_2$ , respectively. At each field, the fixed delay  $\tau$  was

selected to be a multiple of the time interval equivalent to the inverse of the  $^1\text{H}$  Larmor frequency, in order to selectively suppress contributions from solvent matrix protons. The time domain data was baseline-corrected (third-order polynomial) to eliminate the exponential decay in the echo intensity, apodized with a Hamming window function, zero-filled to eight-fold points, and fast Fourier-transformed to yield the 2-dimensional frequency domain. For  $^2\text{H}$ - $^1\text{H}$  difference spectra, the time domain of the HYSORE spectrum of the  $^1\text{H}$  sample was subtracted from that of the  $^2\text{H}$  sample, and the same data processing procedure detailed above was used to generate the frequency spectrum.

In general, the ENDOR spectrum for a given nucleus with spin  $I = \frac{1}{2}$  ( $^1\text{H}$ ) coupled to the  $S = \frac{1}{2}$  electron spin exhibits a doublet at frequencies

$$\nu_{\pm} = \left| \frac{A}{2} \pm \nu_N \right| \quad (\text{S1})$$

Where  $\nu_N$  is the nuclear Larmor frequency and  $A$  is the hyperfine coupling. For nuclei with  $I \geq 1$  ( $^{14}\text{N}$ ,  $^2\text{H}$ ), an additional splitting of the  $\nu_{\pm}$  manifolds is produced by the nuclear quadrupole interaction (P)

$$\nu_{\pm, m_I} = \left| \nu_N \pm \frac{3P(2m_I - 1)}{2} \right| \quad (\text{S2})$$

In HYSORE spectra, these signals manifest as cross-peaks or ridges in the 2-D frequency spectrum which are generally symmetric about the diagonal of a given quadrant. This technique allows hyperfine levels corresponding to the same electron-nuclear submanifold to be differentiated, as well as separating features from hyperfine couplings in the weak-coupling regime ( $|A| < 2|\nu_I|$ ) in the (+,+) quadrant from those in the strong coupling regime ( $|A| > 2|\nu_I|$ ) in the (-,+) quadrant. The (-,-) and (+,-) quadrants of these frequency spectra are symmetric to the (+,+)

and (-,+) quadrants, thus typically only two of the quadrants are typically displayed in literature. For systems with appreciable hyperfine anisotropy in frozen solutions or solids, HYSCORE spectra typically do not exhibit sharp cross peaks, but show ridges that represent the sum of cross peaks from selected orientations at the magnetic field position at which the spectrum is collected. The length and curvature of these correlation ridges allow for the separation and estimation of the magnitude of the isotropic and dipolar components of the hyperfine tensor, as shown in Fig. S1.

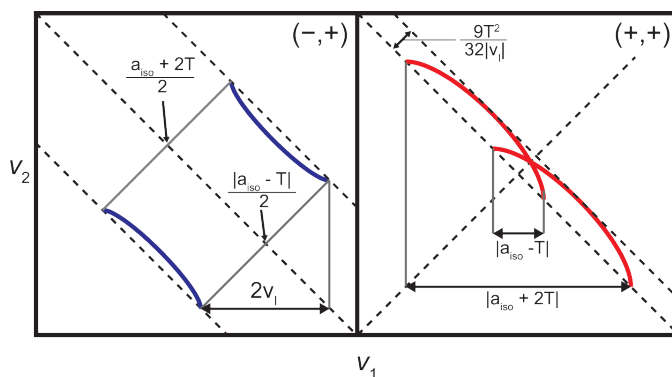


**Figure S1:** HYSCORE powder patterns for an  $S = 1/2$ ,  $I = 1/2$  spin system with an axial hyperfine tensor which contains isotropic ( $a_{iso}$ ) and dipolar ( $T$ ) contributions. Blue correlation ridges represent the strong coupling case; red correlation ridges represent the weak coupling case.

For systems exhibiting significant rhombic symmetry in the hyperfine tensor, as is the case for the  $N_\alpha$  for  $[^{Ar}P_3BFe(NNH_x)]^{-/0/+}$  ( $x = 0, 1, 2$ ), such simple analysis of these correlation ridges is less facile, and even cursory analysis requires spectral simulations.

For systems coupled to nuclei with  $I = 1$ , such as  $^{14}N$ , the double-quantum peaks are often the most intense feature. These cross-peaks are defined by the following equations:

$$v_\alpha = \pm 2 \sqrt{(v_I + A/2)^2 + K^2(3 + \eta^2)} \quad (S3)$$

$$\nu_\beta = \pm 2\sqrt{(v_I - A/2)^2 + K^2(3 + \eta^2)}$$

where  $K = e^2qQ/4\hbar$ . For weakly coupled nuclei ( $A < 2\nu_I$ ),  $\nu_\alpha$  and  $\nu_\beta$  are both positive, appearing in the (+,+) quadrant, while for strongly coupled nuclei they will show up in the (-,+) quadrant. In the intermediate coupling regime where  $A \approx 2\nu_I$ , peaks will often appear in both the (+,+) and (-,+) quadrants of the HYSORE spectrum.

All EPR spectra (CW, ENDOR, HYSORE) were simulated using the EasySpin simulation toolbox (version 5.2.16) with Matlab 2016<sup>7</sup> using the following Hamiltonian:

$$\hat{H} = \mu_B \vec{B}_0 g \hat{S} + \mu_N g_N \vec{B}_0 \hat{I} + h \hat{S} \cdot \mathbf{A} \cdot \hat{I} + h \hat{I} \cdot \mathbf{P} \cdot \hat{I} \quad (\text{S4})$$

In this expression, the first term corresponds to the electron Zeeman interaction term where  $\mu_B$  is the Bohr magneton,  $g$  is the electron spin g-value matrix with principle components  $g = [g_{xx} \ g_{yy} \ g_{zz}]$ , and  $\hat{S}$  is the electron spin operator; the second term corresponds to the nuclear Zeeman interaction term where  $\mu_N$  is the nuclear magneton,  $g_N$  is the characteristic nuclear g-value for each nucleus (e.g.  $^1\text{H}, ^2\text{H}, ^{31}\text{P}$ ) and  $\hat{I}$  is the nuclear spin operator; the third term corresponds to the electron-nuclear hyperfine term, where  $\mathbf{A}$  is the hyperfine coupling tensor with principle components  $\mathbf{A} = [A_{xx}, A_{yy}, A_{zz}]$ ; and for nuclei with  $I \geq 1$ , the final term corresponds to the nuclear quadrupole (NQR) term which arises from the interaction of the nuclear quadrupole moment with the local electric field gradient (efg) at the nucleus, where  $\mathbf{P}$  is the quadrupole coupling tensor. In the principle axis system (PAS),  $\mathbf{P}$  is traceless and parametrized by the quadrupole coupling constant  $e^2Qq/h$  and the asymmetry parameter  $\eta$  such that:

$$\mathbf{P} = \begin{pmatrix} P_{xx} & 0 & 0 \\ 0 & P_{yy} & 0 \\ 0 & 0 & P_{zz} \end{pmatrix} = \frac{e^2 Qq/h}{4I(2I-1)} \begin{pmatrix} -(1-\eta) & 0 & 0 \\ 0 & -(1+\eta) & 0 \\ 0 & 0 & 2 \end{pmatrix} \quad (\text{S5})$$

Where  $\frac{e^2 Qq}{h} = 2I(2I-1)P_{zz}$  and  $\eta = \frac{P_{xx}-P_{yy}}{P_{zz}}$ . The asymmetry parameter may have values between 0 and 1, with 0 corresponding to an electric field gradient with axial symmetry and 1 corresponding to a fully rhombic efg.

The orientations between the hyperfine and NQI tensor principle axis systems and the g-matrix reference frame are defined by the Euler angles ( $\alpha, \beta, \gamma$ ), with rotations performed within the *zyz* convention where  $\alpha$  rotates *xyz* counterclockwise about *z*-axis to give *x'y'z'*,  $\beta$  rotates *x'y'z'* counterclockwise about *y'*-axis to give *x'',y'',z''*,  $\gamma$  rotates *xyz* counterclockwise about *z''*-axis to give final frame orientation.

**X-Ray Crystallography:** XRD studies were carried out at the Beckman Institute Crystallography Facility on a Bruker AXS KAPPA APEXII diffractometer (Mo  $K\alpha$  radiation) or a Bruker AXS D8 VENTURE (Mo  $K\alpha$  or Cu  $K\alpha$ ). Structures were solved using SHELXS or SHELXT and refined against F2 on all data by full-matrix least squares with SHELXL.<sup>8</sup> The crystals were mounted on mitegen loops under Paratone N oil.

**Electrochemistry.** Electrochemical measurements were carried out using a CD instruments 600B electrochemical analyzer. A freshly-polished glassy carbon electrode was used as the working electrode and a graphite rod was used as the auxiliary electrode. Solutions (THF) of electrolyte (0.1 M tetra-*n*-butylammonium hexafluorophosphate) contained ferrocene (0.1 mM), to serve as an internal reference, and analyte (0.2 mM). All reported potentials are referenced to the ferrocene/ferrocenium couple,  $[\text{Cp}_2\text{Fe}]^+ / \text{Cp}_2\text{Fe}$ .

**DFT Calculations.** Geometry optimizations and frequency calculations were performed using dispersion-corrected density functional theory (DFT-D<sub>3</sub>) using Grimme's dispersion correction.<sup>9</sup> Geometry optimizations and frequency calculations were performed using ORCA version 4.0.1.2 with the TPSS functional, the def2-SVP basis set for C, H, P, B, N, Si and O atoms, and the def2-TZVP basis set for Fe. Frequency calculations were performed on optimized geometries to ensure true minima. EPR parameters (hyperfine couplings, nuclear quadrupole parameters) were calculated using the eprnmr module built into ORCA. Input coordinates were taken from the optimized geometries obtained by the methods described above. These calculations utilized the TPSS function in conjunction with the following basis sets, CP(PPP) for Fe, IGLO-III for P, Si, B, N, and N-H protons (in the case of <sup>A</sup>P<sub>3</sub><sup>B</sup>Fe(NNH) and [<sup>A</sup>P<sub>3</sub><sup>B</sup>Fe(NNH<sub>2</sub>)<sup>+</sup>]. def2-SV(P) was used for all other atoms. The radial integration accuracy was increased for Fe, P, B, Si, and N atoms (IntAcc 7) to help capture core polarization effects. Similar DFT methods have been employed in the calculation of EPR and <sup>57</sup>Fe Mössbauer parameters of a related redox series of [P<sub>3</sub><sup>B</sup>Fe(NNMe<sub>2</sub>)]<sup>+0/-</sup> compounds by our group.<sup>10</sup>

### **Synthetic Procedures**

*bis(3,5-diisopropyl-4-methoxyphenyl)-o-bromophenylphosphine:* Mg turnings (16.6 g, 682.99 mmol) were stirred vigorously under N<sub>2</sub> for 2 hours followed by addition of 400 mL THF and 0.5 mL 1,2-dibromoethane. The suspension was heated to reflux for a period of 1 hour to activate the Mg turnings and then allowed to cool to room temperature. 44.3501 g (163.53 mmol) of 4-bromo-2,6-diisopropylanisole in 25 mL THF was added dropwise via addition funnel to the stirring suspension so that little to no exotherm was observed. The reaction vessel was again heated to reflux for 12 hours and cooled to room temperature. The dark cloudy solution was then added to a solution of 21.0662 g (81.69 mmol) 2-bromophenylphosphorusdichloride in 250 mL THF at

-78 °C dropwise via cannula over 2 hours. After addition was completed the reaction mixture was allowed to stir overnight (10 hours) while slowly warming to room temperature. After overnight stirring 750 mL DI H<sub>2</sub>O was added to the reaction mixture and the solution was transferred to a separatory funnel and extracted with 3 x 400 mL Et<sub>2</sub>O. The combined organic layers were dried with MgSO<sub>4</sub> and filtered. Removal of solvent left a viscous oil. The oil was taken up in HMDSO and allowed to stand at room temperature overnight as white solids crashed out of solution. Further cooling of the mother liquor to -35 °C overnight furnished an additional small crop of white solids. The solids were collected on a frit, washed with HMDSO and dried under vacuum. Yield: 35.09 g, 75.4% Elemental Analysis % C; H; N: Found (Calc): C: 67.23 (67.48); H: 7.78 (7.43); N: -0.06 (0.00) <sup>1</sup>H NMR (400 MHz, C<sub>6</sub>D<sub>6</sub>, 298 K): δ 7.40 (dd, 1H, <sup>3</sup>J<sub>HH</sub> = 7.7, <sup>4</sup>J<sub>HH</sub> = 3.2 Hz), 7.34 (s, 2H), 7.32 (s, 2H), 7.13 (d, 1H, <sup>3</sup>J<sub>HH</sub> = 7.7 Hz), 6.77 (dt, 2H, J<sub>HH</sub> = 53.0, 7.4 Hz), 3.44 (s, 6H), 3.34 (hept, 4H, 7.0 Hz), 1.12 (d, 24H, <sup>3</sup>J<sub>HH</sub> = 6.8 Hz). <sup>31</sup>P{<sup>1</sup>H} NMR (202.4 MHz, C<sub>6</sub>D<sub>6</sub>, 298 K, ppm): δ -3.76 (s), <sup>13</sup>C{<sup>1</sup>H} NMR (101 MHz, C<sub>6</sub>D<sub>6</sub>, 298 K, ppm): δ 156.10, 142.45 (d, J = 7.2 Hz), 141.42, 141.25 (d, J = 15.0 Hz), 134.76, 133.29 (d, J = 2.1 Hz), 132.55 (d, J = 10.7 Hz), 130.7 (d, J = 31 Hz) 130.57 (J = 21.1 Hz), 130.14, 127.47, 61.88, 24.12, 24.07.

*ArP<sub>3</sub>B*: 5.0926 g (8.94 mmol) of *arm* was dissolved in 200 mL Et<sub>2</sub>O and cooled to -78 °C. 6.2 mL <sup>n</sup>BuLi (1.6 M in hexanes) was added dropwise to the reaction mixture causing it to turn golden. The solution was stirred cold for 1 hour and then allowed to warm to room temperature over 1 hour and stirred an additional 30 minutes at room temperature. The solution was then chilled to -78 °C and a solution of B(OMe)<sub>3</sub> (312.4 mg, 3.00 mmol) in Et<sub>2</sub>O (40 mL) was added dropwise and the mixture was allowed to slowly warm to RT overnight. All volatiles were removed from the reaction mixture, leaving a tacky cream colored solid. This solid was suspended in pentane and filtered through Celite, leaving a white solid behind on the Celite pad. The white solid was then

washed with Et<sub>2</sub>O (5 x 30 mL) and the washings were collected and cooled to -78 °C. Solid [HNEt<sup>t</sup>Pr<sub>2</sub>]Cl (504.7 mg, 3.05 mmol) was added to the stirring mixture and the reaction was allowed to slowly warm to RT and stirred overnight. The resulting bright yellow solution was pumped down to a yellow foam. The foam was extracted in pentane, filtered through Celite, concentrated, and stored at -35 °C resulting in the formation of bright yellow crystals of ArP<sub>3</sub><sup>B</sup>. Yield: 2.7241 g (61.7%). Elemental Analysis % C; H; N: Found (Calc): C: 77.54 (77.92); H: 9.18 (8.58); N: -0.02 (0.00) <sup>1</sup>H NMR (300 MHz, C<sub>6</sub>D<sub>6</sub>, 298 K, ppm): δ 7.62 (d, 3H, <sup>3</sup>J<sub>HH</sub> = 7.4 Hz), 7.26 (s, br, 12H), 7.12 (d, 3H, <sup>3</sup>J<sub>HH</sub> = 7.4 Hz), 6.81 (dt, 6H, J<sub>HH</sub> = 79.7, 7.6 Hz), 3.5 (s, 18H), 3.36 (hept, 12H, <sup>3</sup>J<sub>HH</sub> = 5.6 Hz), 1.16 (t, 72H, <sup>3</sup>J<sub>HH</sub> 6.8 Hz). <sup>31</sup>P{<sup>1</sup>H} NMR(202.4 MHz, C<sub>6</sub>D<sub>6</sub>, 298 K, ppm) -9.49 (s), <sup>11</sup>B (128 MHz, C<sub>6</sub>D<sub>6</sub>, 298 K, ppm). 3.79 (s, br) <sup>13</sup>C{<sup>1</sup>H} NMR (101 MHz, CDCl<sub>3</sub>, 298 K, ppm) δ 154.22, 142.73 (m), 140.22, 135.47, 134.81 (m), 129.84 (d, J = 7.3 Hz), 129.71 (d, J = 7.7 Hz), 128.94, 128.46, 126.51, 62.28, 26.52, 24.28, 23.93

*ArP<sub>3</sub><sup>B</sup>FeBr*: ArP<sub>3</sub><sup>B</sup> (504.7 mg, 0.34 mmol) and FeBr<sub>2</sub> (79.4mg, 0.37 mmol) were stirred in THF (ca. 10 mL) until all solids had dissolved giving a clear yellow solution. All volatiles were removed and the resulting solid was triturated in Et<sub>2</sub>O and evacuated to dryness. The resulting solid was then dissolved in benzene and combined with Na/Hg amalgam and stirred vigorously overnight giving a dark red-brown solution. The solution was filtered through Celite and all volatiles were removed *in vacuo*, giving a dark brown solid. This solid was dissolved in pentane and allowed to stand at room temperature overnight while tan solids precipitated from solution. The dark brown mother liquor was decanted and filtered through Celite and concentrated and stored at -35 °C, giving ArP<sub>3</sub><sup>B</sup>FeBr as a dark brown microcrystalline powder. Yield: 324.5 mg (58.9 %). X-ray diffraction quality crystals were obtained by slow vapor diffusing from a pentane solution of ArP<sub>3</sub><sup>B</sup>FeBr into HMDSO. Elemental Analysis % C; H; N: Found (Calc): C: 71.78 (71.73); H: 8.35

(7.86); N: 0.03 (0.00)  $^1\text{H}$  NMR (300 MHz,  $\text{C}_6\text{D}_6$ , 298 K, ppm):  $\delta$  30.19 (s, br), 25.03 (s, br), 9.80 (s, br), 3.95 (s, br), 3.45 (s, br), 3.31 (s, br), 2.41 (s, br), 1.46 (s, br), 0.85 (s, br), 0.75 (s, br), -2.06 (s, br), -24.14 (s, br).  $\mu_{\text{eff}}$  ( $\text{C}_6\text{D}_6$ , 298 K, 300 MHz):  $3.7\mu\text{B}$

$^{Ar}\text{P}_3^{B}\text{Fe}(\text{N}_2)$ :  $^{Ar}\text{P}_3^{B}\text{FeBr}$  (142.9 mg, 0.088 mmol) was dissolved in benzene and stirred vigorously over excess sodium amalgam (2.3 equiv.) for 12 hours resulting in formation of a dark forest green solution. The solution was filtered through Celite and volatiles were removed *in vacuo*. The resulting dark forest green solids were extracted in pentane, filtered through Celite again, concentrated, and stored in a freezer at  $-35\text{ }^\circ\text{C}$ , giving  $^{Ar}\text{P}_3^{B}\text{Fe}(\text{N}_2)$  as a dark microcrystalline solid. X-ray diffraction quality crystals were obtained by slow vapor diffusion from a pentane solution of  $^{Ar}\text{P}_3^{B}\text{Fe}(\text{N}_2)$  into HMDSO. Yield: 109.2 mg (79.5 %). Elemental Analysis % C; H; N: Found (Calc): C: 74.16 (73.74); H: 8.50 (8.12); N: 1.69 (1.79).  $^1\text{H}$  NMR (400 MHz,  $\text{C}_6\text{D}_6$ )  $\delta$  7.37 (s, br, 9H), 6.94-6.49 (m, br, 15H), 3.50 (s, 9H), 3.41-3.29 (m, br, 15H), 3.11 (m, br, 6H), 1.27 (s, br, 18H), 1.14 (s, br, 18H), 1.03 (d,  $^3J_{\text{HH}} = 6.8\text{ Hz}$ , 18H), 0.96 (s, br, 18H).  $^{31}\text{P}$  NMR  $\{^1\text{H}\}$  NMR (202.4 MHz,  $\text{C}_6\text{D}_6$ , 298 K, ppm) 79.07 (s, br, 2P), 20.25 (s, br, 1P).  $^{11}\text{B}$  (128 MHz,  $\text{C}_6\text{D}_6$ , 298 K, ppm) 16.08 (s, br). IR (thin film from  $\text{C}_6\text{D}_6$ , 298 K)  $\nu_{\text{N}_2} = 2016\text{ cm}^{-1}$ .

$[^{Ar}\text{P}_3^{B}\text{Fe}(\text{N}_2)][\text{Na}(12\text{-C-4})_2]$ :  $^{Ar}\text{P}_3^{B}\text{Fe}(\text{N}_2)$  (181.1 mg, 0.116 mmol) was dissolved in THF (ca. 7 mL) and stirred vigorously over excess sodium amalgam (5 equiv.) for 12 hours, resulting in formation of a dark red solution. The solution was filtered through Celite and volatiles were removed *in vacuo*. The resulting dark red solids were extracted in  $\text{Et}_2\text{O}$ , and filtered through Celite again and neat 12-crown-4 (40  $\mu\text{L}$ , 0.247 mmol) was added. The solution was allowed to stand for 10 minutes and then was concentrated, layered with pentane, and stored in a freezer at  $-35\text{ }^\circ\text{C}$ , yielding  $[^{Ar}\text{P}_3^{B}\text{Fe}(\text{N}_2)][\text{Na}(12\text{-C-4})_2]$  as a dark red microcrystalline solid. This solid was then washed with pentane until the washings came out colorless (typically 3-5 x 1 mL washes). (note:

Et<sub>2</sub>O and Pentane were additionally dried by passage through a short pipette column of activated alumina prior to use). Yield: 203.0 mg (0.105 mmol, 90 %). Elemental Analysis % C; H; N: Found (Calc): C: 69.04 (69.38); H: 8.19 (8.21); N: 0.39 (1.44). Note: The N content of samples prepared for elemental analysis was consistently low while remaining within acceptable limits on C and H. This is consistent with a labile N<sub>2</sub> ligand, additional evidence of the lability of the N<sub>2</sub> ligand was observed in the rapid exchange of <sup>15</sup>N<sub>2</sub> for <sup>14</sup>N<sub>2</sub> in solution at low temperatures and even in the solid state. <sup>1</sup>H NMR (300 MHz, C<sub>6</sub>D<sub>6</sub>) δ 11.82 (s, br), 10.01 (s, br), 3.75-2.78 (multiple broad overlapping signals), 1.85 (s, br), 1.70-0.70 (multiple broad overlapping signals), -1.36 (s, br). μ<sub>eff</sub> (C<sub>6</sub>D<sub>6</sub>, 298 K, 300 MHz): 1.7 μB. IR(thin film from THF, 298 K) ν<sub>N<sub>2</sub></sub> = 1937 cm<sup>-1</sup>.

[<sup>Ar</sup>P<sub>3</sub><sup>B</sup>Fe(<sup>15</sup>N<sub>2</sub>)][Na(12-C-4)<sub>2</sub>]: A Schlenk round bottom flask was loaded with <sup>Ar</sup>P<sub>3</sub><sup>B</sup>FeBr (379.6 mg, 0.235 mmol) and Na/Hg amalgam (3.9 equiv.). The round bottom was evacuated and THF (ca. 10 mL) was vacuum transferred into the flask following thorough degassing via 5 freeze-pump-thaw cycles. <sup>15</sup>N<sub>2</sub> (2.1 equiv.) was introduced from a calibrated bulb and the solution was allowed to thaw slowly while stirring for 12 hours, resulting in formation of a dark red solution. The solution was filtered via cannula under argon and volatiles were removed *in vacuo*. The resulting dark red solids were extracted in a solution of Et<sub>2</sub>O (5mL) containing 12-crown-4 (300 μL, 7.9 equiv.). The solution was allowed to stand for 10 minutes and then was layered with pentane, and stored in a freezer at -35 °C, yielding [<sup>Ar</sup>P<sub>3</sub><sup>B</sup>Fe(<sup>15</sup>N<sub>2</sub>)][Na(12-C-4)<sub>2</sub>] as a dark red solid. This solid was then washed with pentane (3 x 5 mL washes). (note: Et<sub>2</sub>O and Pentane were additionally dried by passage through a short pipette column of activated alumina and degassed via three freeze-pump-thaw cycles prior to use). Yield: ca. 300 mg (65.8%). <sup>1</sup>H NMR spectra of sample prepared under argon were identical to [<sup>Ar</sup>P<sub>3</sub><sup>B</sup>Fe(<sup>15</sup>N<sub>2</sub>)][Na(12-C-4)<sub>2</sub>]. IR spectra collected under an atmosphere of N<sub>2</sub> either of an evaporated thin film or of solid material showed no

isotopically shifted N-N stretch due to rapid exchange of the  $^{15}\text{N}_2$  ligand with  $\text{N}_2$  in the glovebox atmosphere. Incorporation of  $^{15}\text{N}$  was nonetheless verified via the clear changes in HYSORE spectra, where the loss of  $^{14}\text{N}$  features was accompanied by new signals centered at the Larmor frequency for  $^{15}\text{N}$ . Note: Due to the rapid exchange of the  $\text{N}_2$  ligand with atmospheric  $\text{N}_2$ , isotopic enrichment with  $^{15}\text{N}_2$  can also be achieved by allowing samples of  $[\text{ArP}_3^{\text{B}}\text{Fe}(\text{N}_2)][\text{Na}(12\text{-C-4})_2]$  to incubate in solution under an excess of  $^{15}\text{N}_2$  in a sealed vessel for several minutes (vide infra).

*ArP<sub>3</sub><sup>B</sup>Fe(NNSiMe<sub>3</sub>):* 81.2 mg (50.2  $\mu\text{mol}$ )  $\text{ArP}_3^{\text{B}}\text{FeBr}$  and 7.0  $\mu\text{L}$  (55.0  $\mu\text{mol}$ )  $\text{Me}_3\text{SiCl}$  were combined in ca. 7 mL THF. Freshly prepared 1% Na/Hg (3.0 equiv.) was added and the mixture was stirred vigorously for 3 hours) resulting in a dark red-brown solution. Volatiles were removed *in vacuo* and the reaction mixture was stirred vigorously in ca. 7 mL benzene for an additional 3 hours giving a dark green-brown solution. This solution was filtered through Celite and lyophilized, giving a fine dark green-brown powder. Yield 77.2 mg (94.0 %).  $^1\text{H}$  NMR (300 MHz,  $\text{C}_6\text{D}_6$ )  $\delta$  11.31 (s, br), 3.23 (s, br), 2.93 (s, br), 2.63 (s, br), 0.68 (s, br), -0.97 (s, br), -2.33 (s, br). (note: this compound is nearly NMR silent at 25  $^\circ\text{C}$  and signals can only be clearly observed in very concentrated solutions ( $\sim 120$  mM). This compound slowly decomposes over time in solution and in the solid state to give  $\text{ArP}_3^{\text{B}}\text{Fe}(\text{N}_2)$  and hexamethyldisilane and attempts to crystallize this compound resulted in near quantitative recovery of  $\text{ArP}_3^{\text{B}}\text{Fe}(\text{N}_2)$ . However, the IR spectra of freshly prepared samples generated by the above method show either no component or a very small component of  $\text{ArP}_3^{\text{B}}\text{Fe}(\text{N}_2)$ . Additionally, no other species were detected in the crude material by  $^1\text{H}$  or  $^{31}\text{P}$  NMR. As such this material is best used freshly prepared and purity should be evaluated by IR,  $^1\text{H}$  and  $^{31}\text{P}$  spectroscopies. IR(thin film from  $\text{C}_6\text{H}_6$ , 298 K)  $\nu_{\text{NN}} = 1717 \text{ cm}^{-1}$ .

*Generation of ArP<sub>3</sub><sup>B</sup>Fe(NNH):* In a typical experiment 5.4 mg (2.8  $\mu\text{mol}$ ) of  $[\text{ArP}_3^{\text{B}}\text{Fe}(\text{N}_2)][\text{Na}(12\text{-C-4})_2]$  was dissolved in 150  $\mu\text{L}$  2-MeTHF and transferred into a 4 mm

diameter quartz EPR tube and frozen in the glovebox cold well cooled with a liquid nitrogen bath. 2.9 mg HBar<sup>F</sup><sub>24</sub> (2.9 μmol) was dissolved in 150 μL thawing 2-MeTHF and the acid solution was layered into the EPR tube and allowed to freeze. The two layers were then mechanically mixed for a period of 30 minutes with a stainless steel needle in the EPR tube, keeping intermittent contact with the chilled sides of the cold well to keep the solutions at or near -135 °C. The resulting brown solutions were then analyzed by EPR spectroscopic methods. Alternative preparations using excesses of HBar<sup>F</sup><sub>24</sub> (up to 5 equivalents) and HOTF (up to 20 equivalents) yielded identical spectroscopic signatures as judged by CW-X-band EPR. Isotopically enriched samples (<sup>2</sup>H) were prepared by appropriately substituting DBar<sup>F</sup><sub>24</sub> in the above procedure.

*Generation of <sup>Ar</sup>P<sub>3</sub><sup>B</sup>Fe(<sup>15</sup>N<sup>15</sup>NH):* In a typical experiment, 5.4 mg (2.8 μmol) of [<sup>Ar</sup>P<sub>3</sub><sup>B</sup>Fe(N<sub>2</sub>)][Na(12-C-4)<sub>2</sub>] was dissolved in 150 μL 2-MeTHF and transferred into a 4 mm diameter quartz EPR tube fitted with a J-Young gas-tight valve. The solution was degassed via four freeze-pump-thaw cycles and charged with 50-100 equivalents of <sup>15</sup>N<sub>2</sub> gas. The tube was then sealed and the solution was allowed to stand for 30 minutes. The solution was then frozen in a liquid nitrogen cooled cold well inside the glove box. Once frozen, the seal was broken and 6.0 mg HBar<sup>F</sup><sub>24</sub> (5.9 μmol) was dissolved in 150 μL thawing 2-MeTHF and the acid solution was layered into the EPR tube and allowed to freeze. The two layers were then mechanically mixed for a period of 30 minutes with a stainless steel needle in the EPR tube keeping intermittent contact with the chilled sides of the cold well to keep the solutions at or near -135 °C. The resulting brown solutions were then analyzed by EPR spectroscopic methods.

*Generation of [<sup>Ar</sup>P<sub>3</sub><sup>B</sup>Fe(NNH<sub>2</sub>)][Bar<sup>F</sup><sub>24</sub>]:* In a typical experiment 5.4 mg (2.8 μmol) of [<sup>Ar</sup>P<sub>3</sub><sup>B</sup>Fe(N<sub>2</sub>)][Na(12-C-4)<sub>2</sub>] was dissolved in 150 μL 2-MeTHF and transferred into a 4 mm diameter quartz EPR tube and frozen in the glovebox cold well cooled with a liquid nitrogen bath.

6.0 mg HBAr<sup>F</sup><sub>24</sub> (5.9 μmol) was dissolved in 150 μL thawing 2-MeTHF and the acid solution was layered into the EPR tube and allowed to freeze. The two layers were then mechanically mixed for a period of 15 minutes with a stainless steel needle in the EPR tube, keeping intermittent contact with the chilled sides of the cold well to keep the solutions at or near -135 °C. The resulting brown solutions were then warmed to -78 °C for 3 minutes, flash frozen in liquid N<sub>2</sub>, and analyzed by EPR spectroscopic methods. Alternative preparations using excesses of HBAr<sup>F</sup><sub>24</sub> (up to 5 equivalents) yielded identical spectroscopic signatures as judged by CW-X-band EPR. Isotopically enriched samples (<sup>2</sup>H or <sup>15</sup>N) were prepared by appropriately substituting DBAr<sup>F</sup><sub>24</sub> or [<sup>A</sup>rP<sub>3</sub><sup>B</sup>Fe(<sup>15</sup>N<sub>2</sub>)] [Na(12-C-4)<sub>2</sub>] in the above procedure.

**Table S1:** XRD experimental parameters for  ${}^{\text{Ar}}\text{P}_3^{\text{B}}\text{FeBr}$ ,  $({}^{\text{Ar}}\text{P}_3^{\text{B}})\text{Fe}(\text{N}_2)$ 

Compound	${}^{\text{Ar}}\text{P}_3^{\text{B}}\text{FeBr}$	${}^{\text{Ar}}\text{P}_3^{\text{B}}\text{Fe}(\text{N}_2)$
Chemical Formula	$\text{C}_9\text{H}_{126}\text{BO}_6\text{P}_3\text{FeBr}$	$\text{C}_9\text{H}_{126}\text{Fe}(\text{N}_2)\cdot\text{C}_5\text{H}_{12}$
Formula Weight	1615.44	1635.70
$T$ (K)	100(2)K	100(2)K
$\lambda$ (Å)	1.54178	0.71073
Space Group	P-1	P-1
A	13.3439(11)	11.8779(8)
B	13.9184(11)	14.7827(9)
C	25.1806(19)	27.0968(17)
A	93.843(5)	86.055(3)
B	90.086(5)	81.569(3)
$\gamma$	109.902(5)	89.245(3)
Volume	4386.0(6)	4695.3(5)
Z	2	2
Density (calc)	1.223	1.157
R1, wr2	0.1122, 0.2874	0.1263, 0.1623

$$\text{R1} = \frac{\sum ||\text{F}_o| - |\text{F}_c||}{\sum |\text{F}_o|}, \text{wR2} = \left\{ \frac{\sum [w(\text{F}_o^2 - \text{F}_c^2)^2]}{\sum w(\text{F}_o^2)^2} \right\}^{1/2}$$

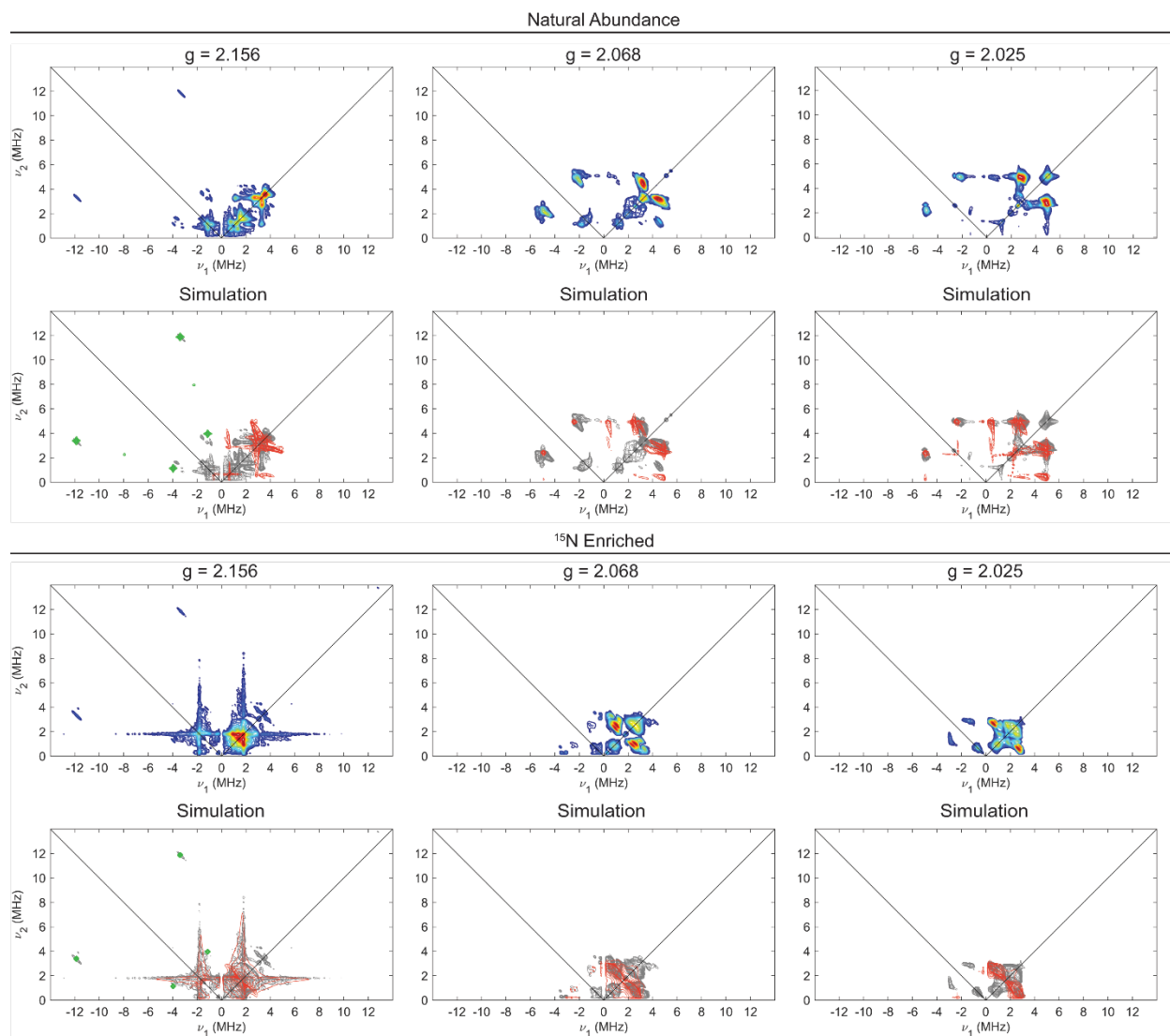


**Figure S2:** Comparison of field-dependent X-band HYSCORE spectra (top panels) and simulations (bottom panels) of  $[\text{ArP}_3\text{BFe}(\text{N}_2)][\text{Na}(12\text{-C-4})_2]$  made with natural abundance  $^{14}\text{N}_2$  (top row) and  $^{15}\text{N}_2$  (bottom row). For simulation panels, experimental data is in grey,  $^{14}\text{N}\alpha$  or  $^{15}\text{N}\alpha$  (red),  $^{11}\text{B}$  (green) using simulation parameters in Table 1 of the main text. Acquisition parameters: temperature = 20 K; magnetic field = 325.3 mT; microwave frequency = 9.411 GHz ( $^{14}\text{N}$ ), 9.424 GHz ( $^{15}\text{N}$ ); MW pulse length ( $\pi/2$ ,  $\pi$ ) = 8 ns, 16 ns;  $\tau$  = 150 ns ( $g = 2.156$ ), 144 ns ( $g = 2.068$ ), 144 ns ( $g = 2.025$ );  $t_1 = t_2 = 100$  ns;  $\Delta t_1 = \Delta t_2 = 16$  ns; shot repetition time (srt) = 1 ms).

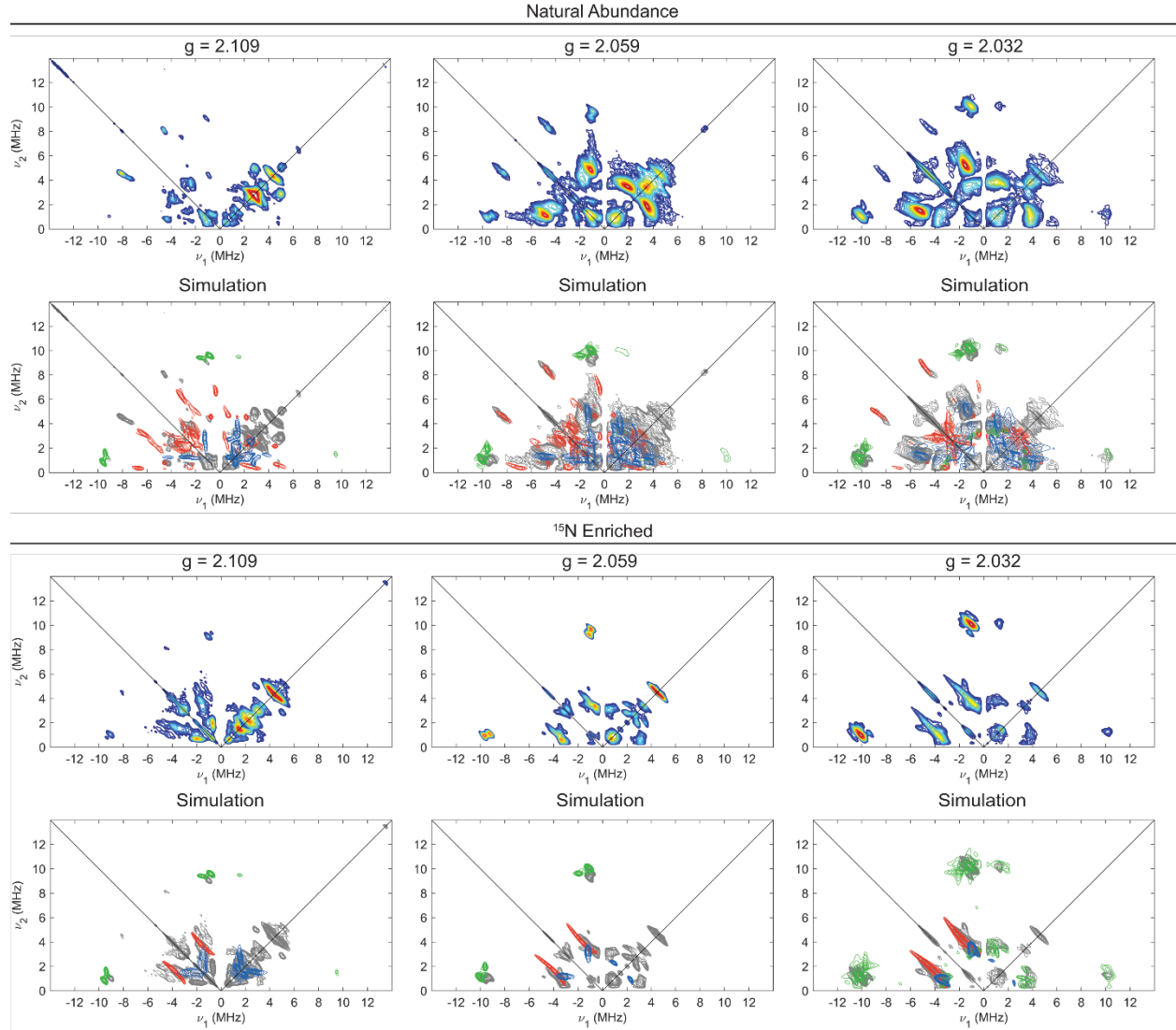


**Figure S3:** Comparison of field-dependent X-band HYSCORE spectra (top panels) and simulations (bottom panels) of  $^{\text{Ar}}\text{P}_3\text{BFe}(\text{NNH})$  made with natural abundance  $^{14}\text{N}_2$  (top row) and  $^{15}\text{N}_2$  (bottom row). For simulation panels, experimental data is in grey,  $^{14}\text{N}\alpha$  or  $^{15}\text{N}\alpha$  (red),  $^{14}\text{N}\beta$  or  $^{15}\text{N}\beta$  (blue) and  $^{11}\text{B}$  (green) using simulation parameters in Table 2 of the main text. Acquisition parameters: Temperature = 20 K; microwave frequency = 9.392 GHz;  $\tau = 148$  ns ( $g = 2.109$ ),  $\tau = 142$  ns ( $g = 2.059$ ); MW pulse length ( $\pi/2$ ,  $\pi$ ) = 8 ns, 16 ns;  $\tau = 142$  ns ( $g = 2.032$ );  $t_1 = t_2 = 100$  ns;  $\Delta t_1 = \Delta t_2 = 16$  ns; shot repetition time (srt) = 1 ms).

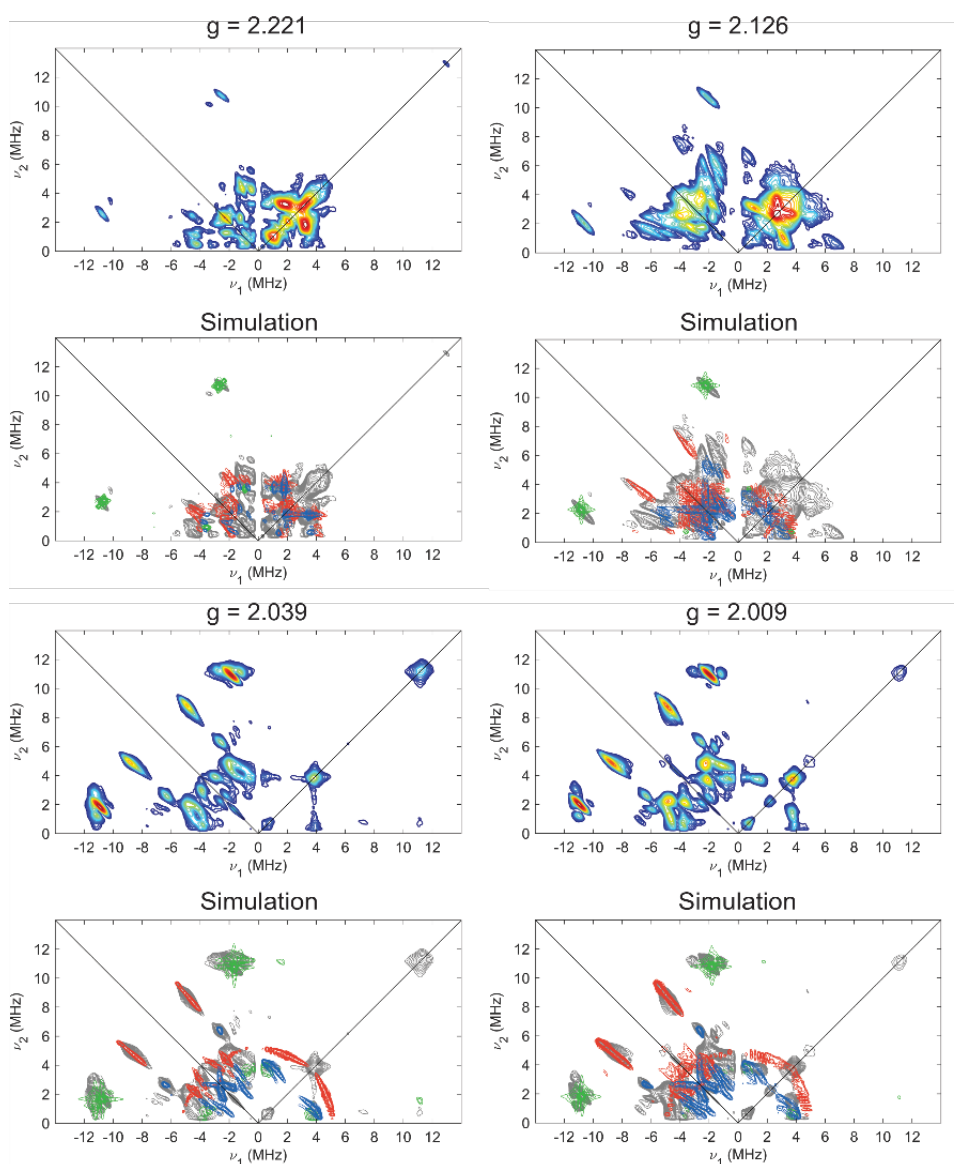


**Figure S4:** Field-Dependent X-Band HYSORE spectra of  ${}^{\text{Ar}}\text{P}_3\text{BFe}(\text{NNSiMe}_3)$  (top) with comparison (bottom) of experimental data (grey) to simulations of  ${}^{14}\text{N}_\alpha$  (red),  ${}^{14}\text{N}_\beta$  (blue) and  ${}^{11}\text{B}$  (green) using simulation parameters in Table 3 of the main text. Acquisition parameters: Temperature = 20 K; microwave frequency = 9.392 GHz ( ${}^{14}\text{N}$ );  $\tau = 148$  ns ( $g = 2.221$ ),  $\tau = 146$  ns ( $g = 2.126$ ); MW pulse length ( $\pi/2, \pi$ ) = 8 ns, 16 ns;  $\tau = 142$  ns ( $g = 2.039$ ),  $\tau = 140$  ns ( $g = 2.009$ );  $t_1 = t_2 = 100$  ns;  $\Delta t_1 = \Delta t_2 = 16$  ns; shot repetition time (srt) = 1 ms.

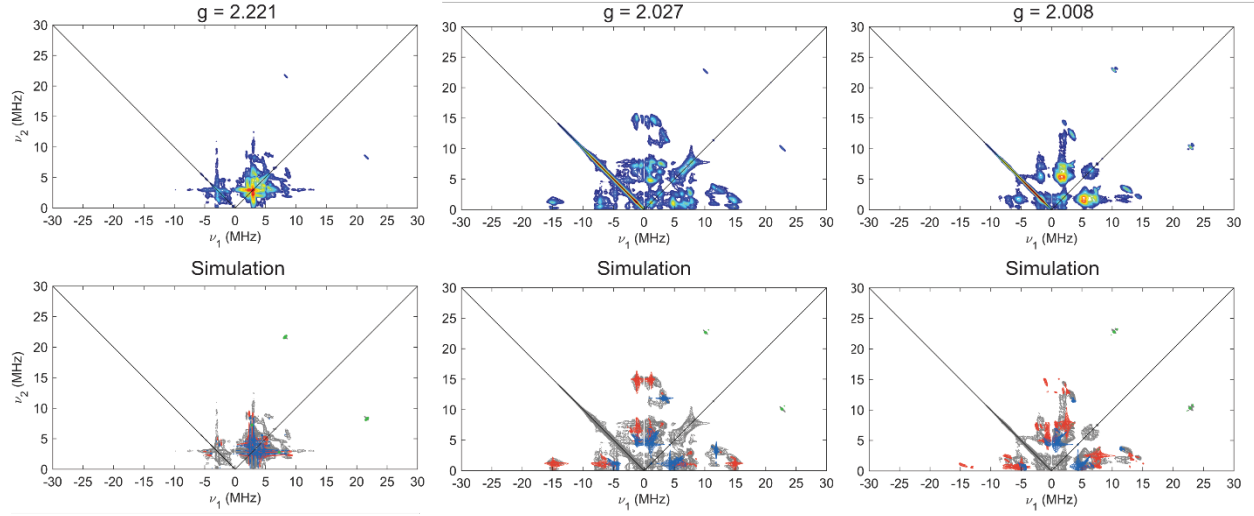


**Figure S5:** Field-Dependent Q-Band HYSCORE spectra of  ${}^{\text{Ar}}\text{P}_3\text{BFe}(\text{NNSiMe}_3)$  (top) with comparison (bottom) of experimental data (grey) to simulations of  ${}^{14}\text{N}_\alpha$  (red),  ${}^{14}\text{N}_\beta$  (blue) and  ${}^{11}\text{B}$  (green) using simulation parameters in Table 3 of the main text. Acquisition parameters: Temperature = 10 K; microwave frequency = 34.040 GHz; MW pulse length ( $\pi/2$ ,  $\pi$ ) = 12 ns, 24 ns;  $\tau = 150$  ns;  $t_1 = t_2 = 100$  ns;  $\Delta t_1 = \Delta t_2 = 16$  ns; shot repetition time (srt) = 2 ms.

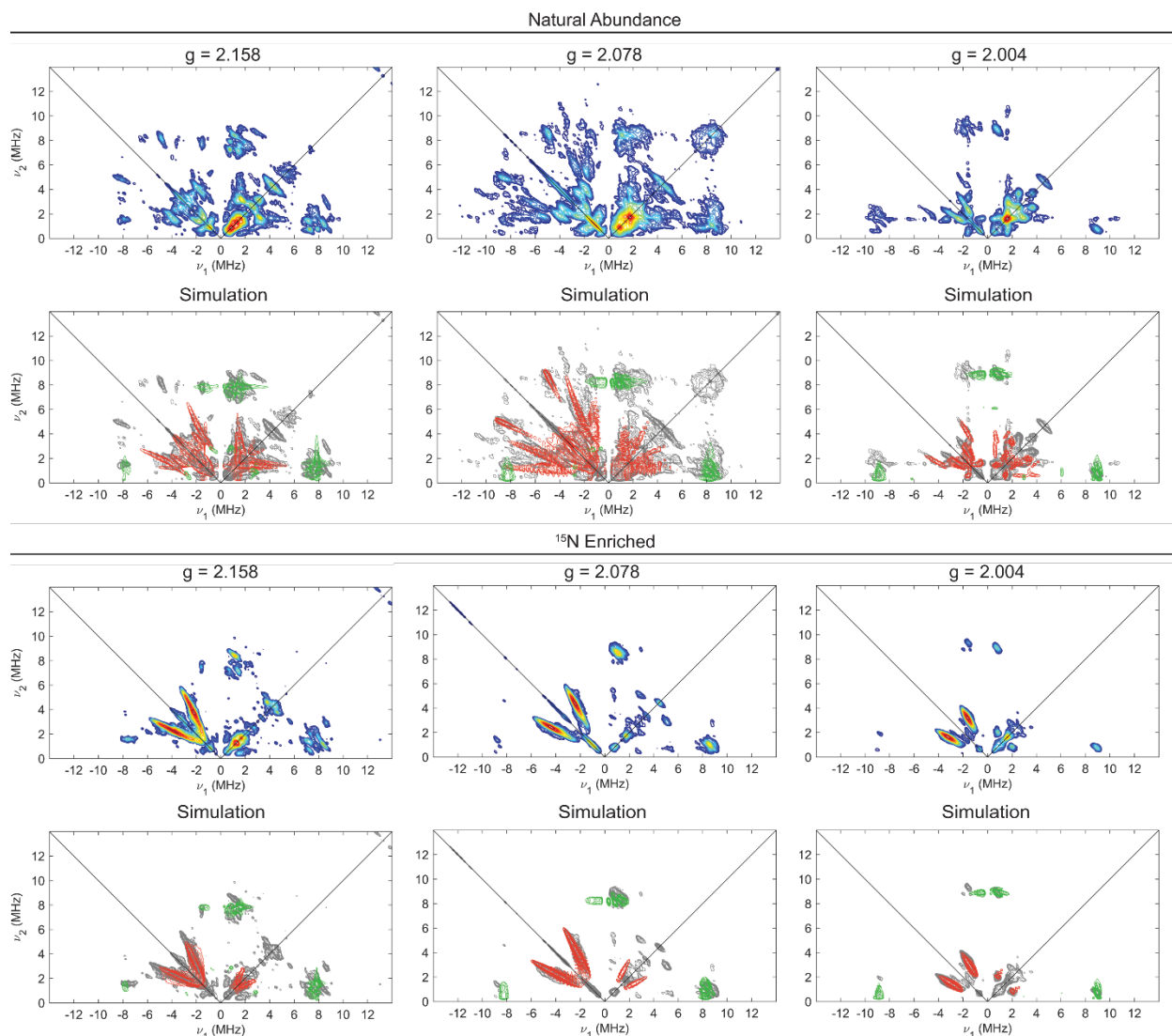


**Figure S6:** Comparison of field-dependent X-band HYSORE spectra (top panels) and simulations (bottom panels) of  $[\text{ArP}_3\text{BFe}(\text{NNH}_2)][\text{BArF}_{24}]$  made with natural abundance  $^{14}\text{N}_2$  (top row) and  $^{15}\text{N}_2$  (bottom row). For simulation panels, experimental data is in grey,  $^{14}\text{N}\alpha$  or  $^{15}\text{N}\alpha$  (red),  $^{11}\text{B}$  (green) using simulation parameters in Table 4 of the main text. Acquisition parameters: temperature = 20 K; microwave frequency = 9.424 GHz ( $^{14}\text{N}$ ), 9.423 GHz ( $^{15}\text{N}$ );  $\tau = 150$  ns ( $g = 2.158$ ); MW pulse length ( $\pi/2, \pi$ ) = 8 ns, 16 ns;  $\tau = 142$  ns ( $g = 2.078$ ),  $\tau = 140$  ns ( $g = 2.004$ );  $t_1 = t_2 = 100$  ns;  $\Delta t_1 = \Delta t_2 = 16$  ns; shot repetition time (srt) = 1 ms.

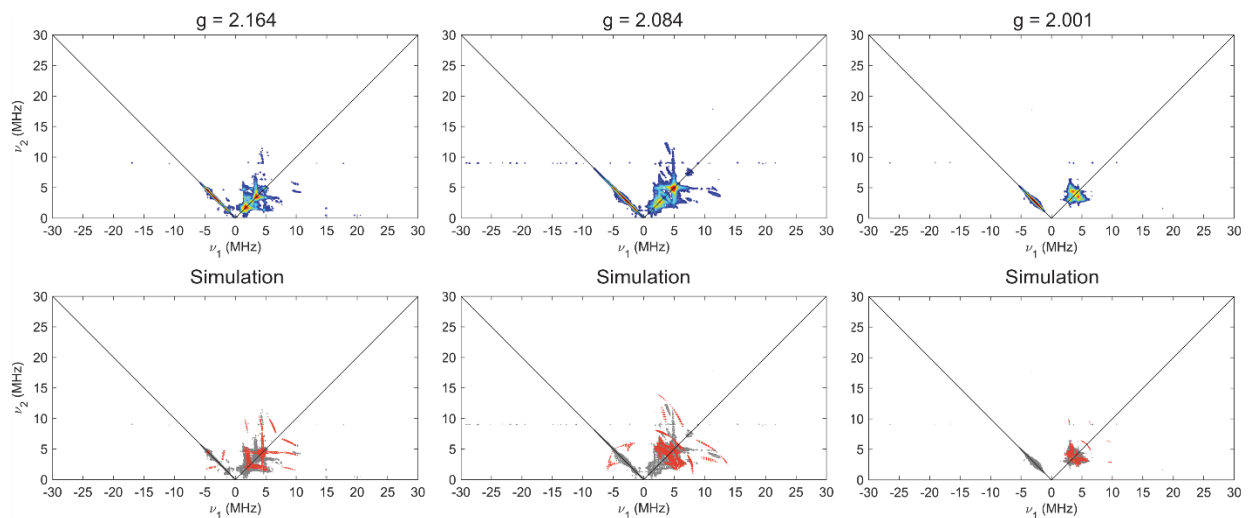


**Figure S7:** Field-dependent Q-band HYSCORE spectra (top panels) and simulations (bottom panels) of  $[\text{ArP}_3\text{BFe}(\text{NNH}_2)][\text{BARF}_{24}]$  made with natural abundance  $^{14}\text{N}_2$ . For simulation panels, experimental data is in grey,  $^{14}\text{N}\alpha$  (red),  $^{11}\text{B}$  (green) using simulation parameters in Table 4 of the main text. Acquisition parameters: temperature = 20 K; microwave frequency = 33.635 GHz; MW pulse length ( $\pi/2$ ,  $\pi$ ) = 12 ns, 24 ns;  $\tau$  = 140 ns;  $t_1 = t_2 = 100$  ns;  $\Delta t_1 = \Delta t_2 = 16$  ns; shot repetition time (srt) = 1 ms.

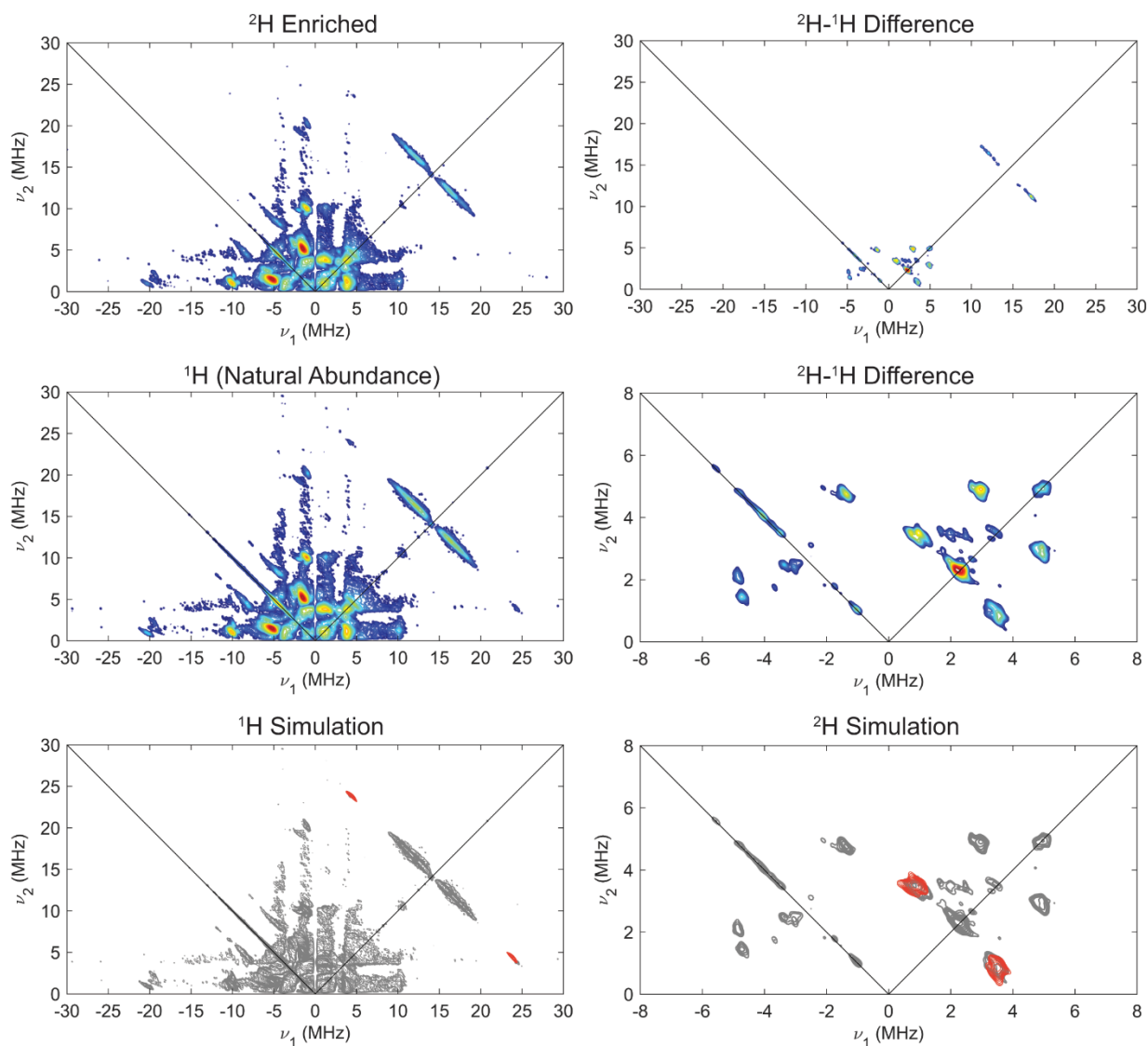


**Figure S8:** Comparison of X-band HYSORE of  $^{\text{Ar}}\text{P}_3^{\text{B}}\text{Fe}(\text{NNH})$  generated with  $\text{DBAr}^{\text{F}_{24}} \cdot 2\text{Et}_2\text{O}$  (top left) and  $\text{HBAr}^{\text{F}_{24}} \cdot 2\text{Et}_2\text{O}$  (middle left) acquired at  $g = 2.032$ . Bottom left: Simulation of the single acid-derived  $^1\text{H}$  coupling (red) of  $A(^1\text{H}) = [19.3, 18.3, 12.0]$  MHz determined via X-band ENDOR (Fig. 7, main text) is superimposed over the natural abundance experimental data (grey). Top right:  $^2\text{H}$  - $^1\text{H}$  difference HYSORE spectrum. Middle right: narrower frequency range of the same difference spectrum. Bottom right: overlay of simulation of acid-derived  $^2\text{H}$  coupling using the same  $^1\text{H}$  coupling scaled by the ratio of  $^2\text{H}/^1\text{H}$  gyromagnetic ratios ( $^2\text{H}\gamma/^1\text{H}\gamma = 0.154$ ) such that  $A(^2\text{H}) = [2.97, 2.82, 1.85]$  MHz, with  $^2\text{H}$  nuclear quadrupole parameters  $e^2Qq/h = 0.25$  MHz and  $\eta = 0.1$ . Acquisition parameters: Temperature = 20 K; microwave frequency = 9.392 GHz; MW pulse length ( $\pi/2, \pi$ ) = 8 ns, 16 ns;  $\tau = 142$  ns;  $t_1 = t_2 = 100$  ns;  $\Delta t_1 = \Delta t_2 = 16$  ns; shot repetition time (srt) = 1 ms).

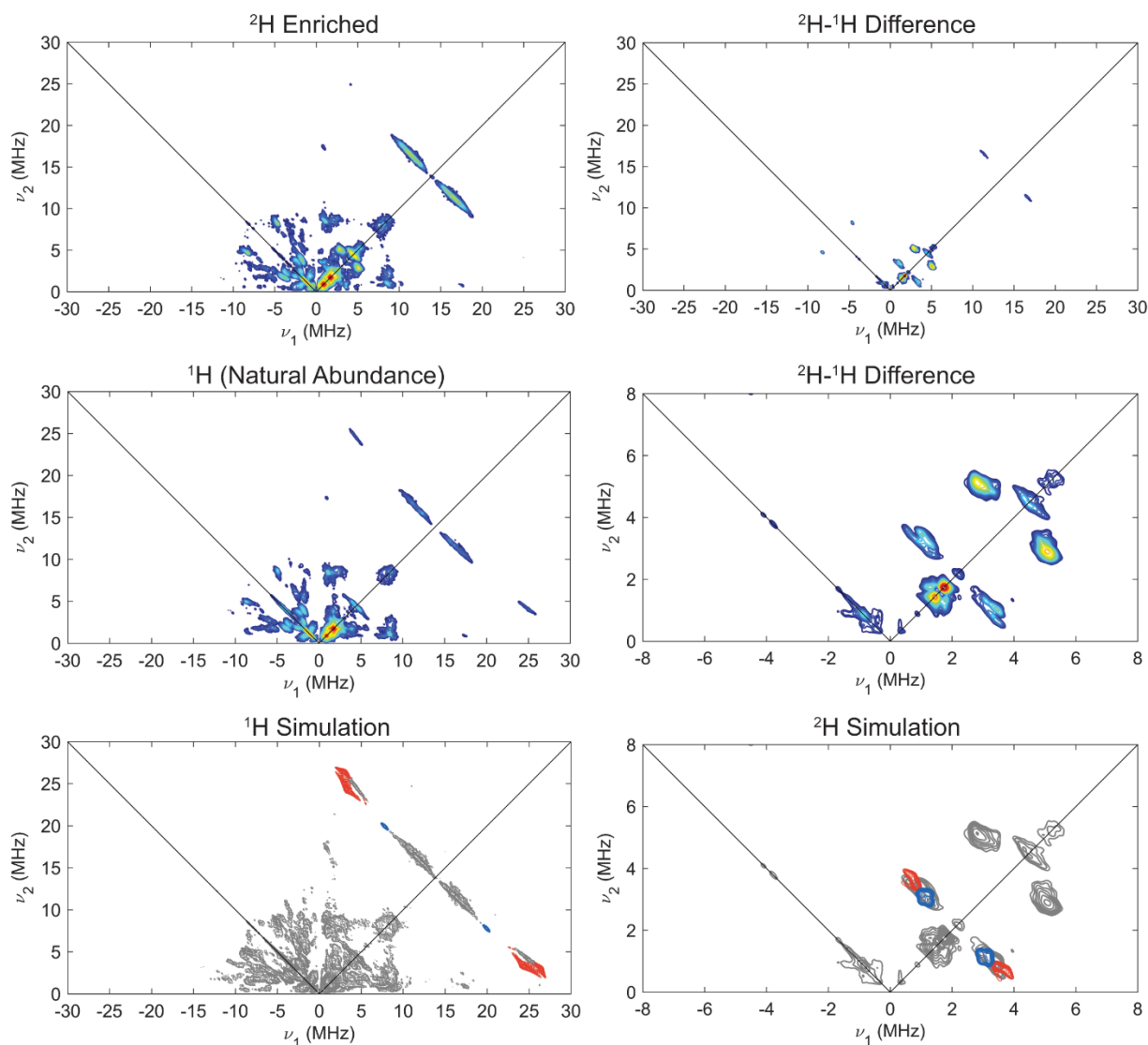


**Figure S9:** Comparison of X-band HYSORE of  $[\text{ArP}_3\text{BFe}(\text{NNH}_2)][\text{BAr}^{\text{F}}_{24}]$  generated with  $\text{DBAr}^{\text{F}}_{24}\cdot 2\text{Et}_2\text{O}$  (top left) and  $\text{HBar}^{\text{F}}_{24}\cdot 2\text{Et}_2\text{O}$  (middle left) acquired at  $g = 2.078$ . Bottom left: Simulation of two acid-derived  $^1\text{H}$  couplings of  $A(^1\text{H}_a) = [16, 21, 27]$  MHz (red) and  $A(^1\text{H}_b) = [10, 13.5, 15]$  MHz (blue) determined via Q-band ENDOR (Fig. 7, main text) are superimposed over the natural abundance experimental data (grey). Top right:  $^2\text{H}$ - $^1\text{H}$  difference HYSORE spectrum. Middle right: narrower frequency range of the same difference spectrum. Bottom right: overlay of simulation of acid-derived  $^2\text{H}$  couplings using the same  $^1\text{H}$  couplings scaled by the ratio of  $^2\text{H}/^1\text{H}$  gyromagnetic ratios ( $^2\text{H}\gamma/^1\text{H}\gamma = 0.154$ ) such that  $A(^2\text{H}_a) = [2.46, 3.23, 4.16]$  MHz (red) and  $A(^2\text{H}_b) = [1.54, 2.08, 2.31]$  MHz (blue). Both  $^2\text{H}_a$  and  $^2\text{H}_b$  were simulated using  $^2\text{H}$  nuclear quadrupole parameters  $e^2Qq/h = 0.25$  MHz and  $\eta = 0.1$ . Acquisition parameters: Temperature = 20 K; microwave frequency = 9.392 GHz; MW pulse length ( $\pi/2, \pi$ ) = 8 ns, 16 ns;  $\tau = 142$  ns;  $t_1 = t_2 = 100$  ns;  $\Delta t_1 = \Delta t_2 = 16$  ns; MW pulse length ( $\pi/2, \pi$ ) = 8 ns, 16 ns; shot repetition time (srt) = 1 ms).

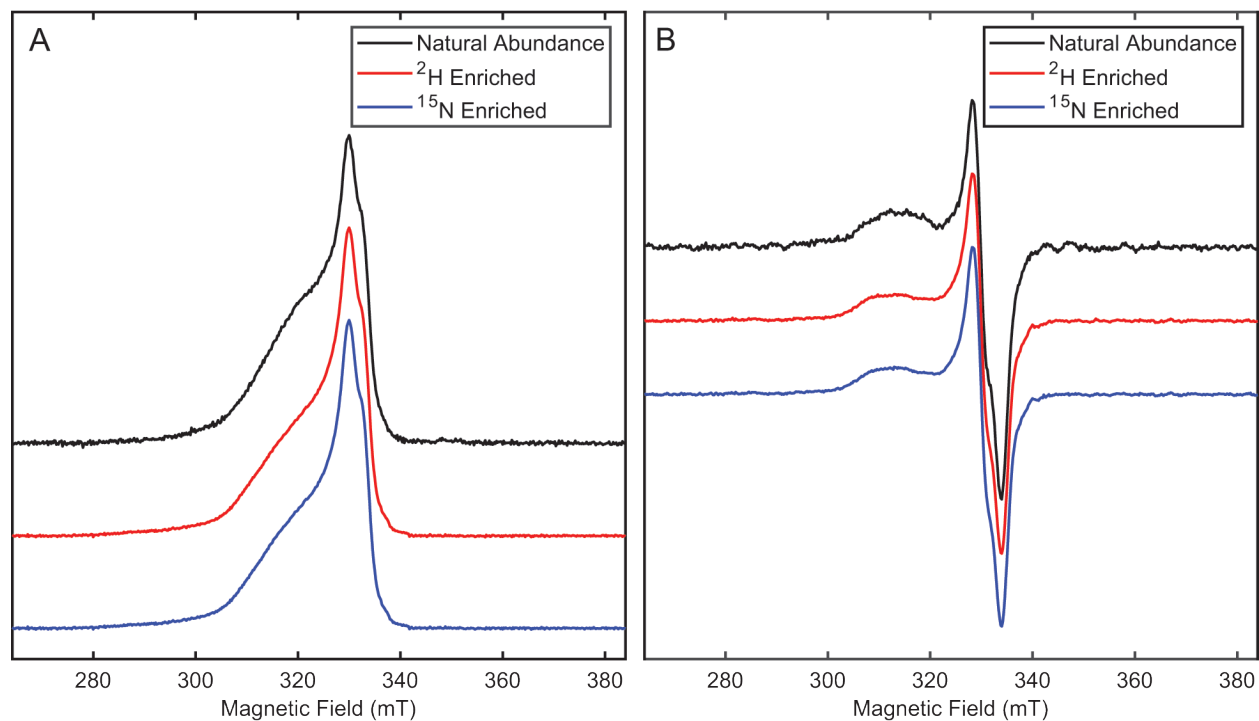


**Figure S10:** A) Comparison of X-band ESE-EPR spectra of natural abundance (black), <sup>2</sup>H enriched (blue), and <sup>15</sup>N enriched <sup>Ar</sup>P<sub>3</sub><sup>B</sup>Fe(NNH). B) Comparison of pseudomodulated (3 mT) X-band ESE-EPR spectra of natural abundance (black), <sup>2</sup>H enriched (blue), and <sup>15</sup>N enriched <sup>Ar</sup>P<sub>3</sub><sup>B</sup>Fe(NNH). Acquisition Parameters: temperature = 20 K; MW Frequency = 9.392 GHz;  $\tau$  = 300 ns; MW pulse length ( $\pi/2$ ,  $\pi$ ) = 80 ns, 160 ns; srt = 1 ms.

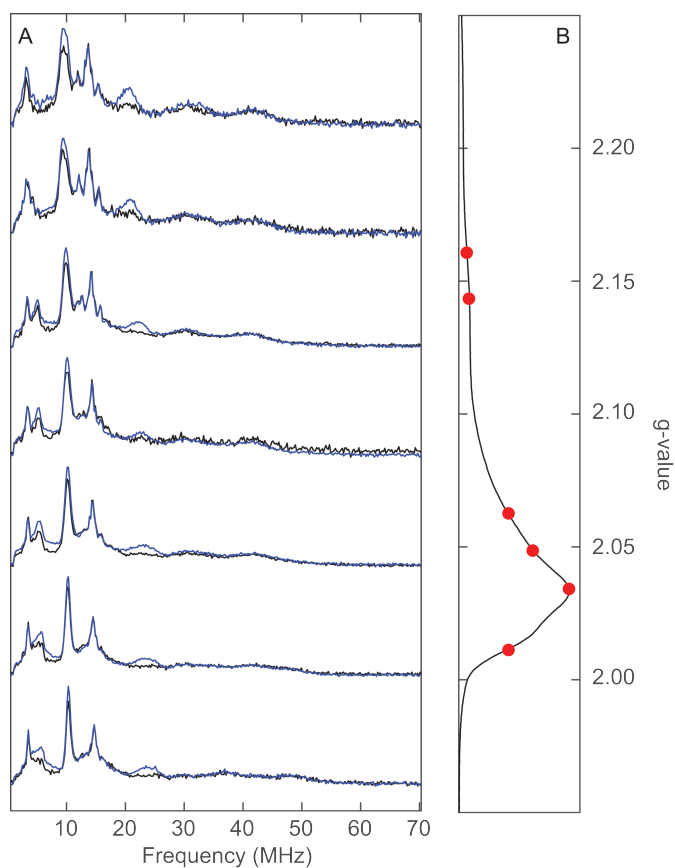


**Figure S11:** Comparison of  $^{Ar}P_3^BFe(NNH)$  (blue trace) and  $^{Ar}P_3^BFe(NND)$  (black trace) X-Band Davies ENDOR spectra (Experimental Parameters: temperature = 10 K; MW Frequency = 9.72 GHz;  $\tau = 240$  ns; MW pulse length ( $\pi/2, \pi$ ) = 20 ns, 40 ns; RF pulse length = 15  $\mu$ s; srt = 5 ms).

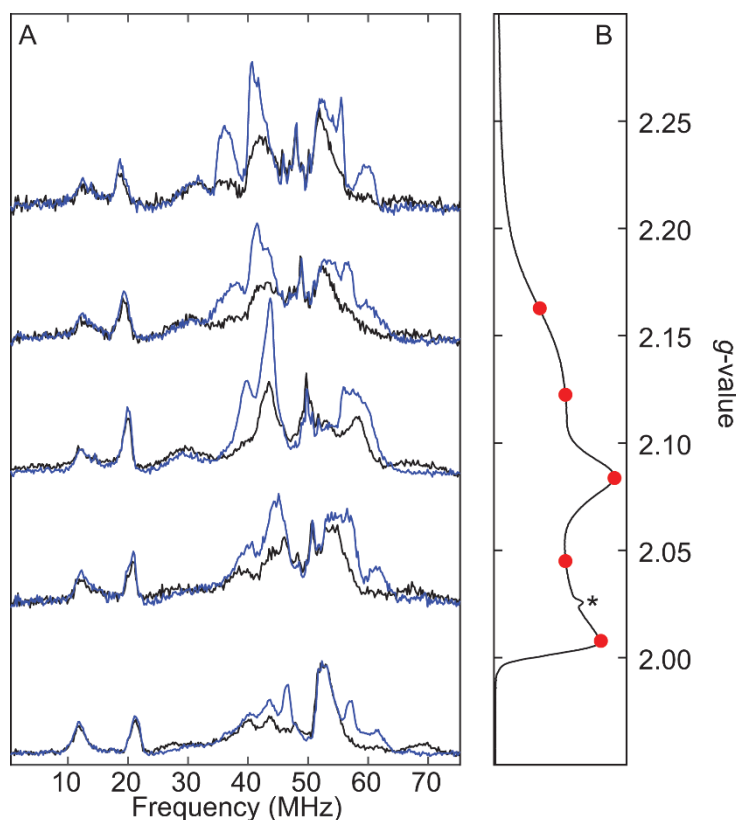


**Figure S12:** A) Field-Dependent Q-Band ENDOR Comparing Spectra of  $[\text{ArP}_3^{\text{B}}\text{Fe}(\text{NNH}_2)][\text{BAR}^{\text{F}}_{24}]$  (blue trace) and  $[\text{ArP}_3^{\text{B}}\text{Fe}(\text{NND}_2)][\text{BAR}^{\text{F}}_{24}]$  (black trace). B) Q-band ESE-EPR spectrum of  $[\text{ArP}_3^{\text{B}}\text{Fe}(\text{NNH}_2)][\text{BAR}^{\text{F}}_{24}]$  with ENDOR acquisition fields indicated with red circles. Asterisk indicates the presence of a background signal arising from a component of the Q-band ENDOR resonator. Experimental Parameters: Temperature = 10 K; MW Frequency = 34.121 GHz;  $\tau = 240$  ns; MW pulse length ( $\pi/2$ ,  $\pi$ ) = 20 ns, 40 ns; RF pulse length = 15  $\mu\text{s}$ ; srt = 5 ms.

**Table S2:**  $^{11}\text{B}$  Nuclear Quadrupole Couplings and Electric Field Gradient Asymmetry Parameters Derived from ENDOR and HYSCORE Spectra.

Compound	$e^2Qq/h$ (MHz)	$\eta$
$[\text{ArP}_3^{\text{B}}\text{Fe}(\text{N}_2)][\text{Na}(12\text{-C-}4)_2]$	0.3	0.1
$\text{ArP}_3^{\text{B}}\text{Fe}(\text{NNH})$	1.0	0.3
$\text{ArP}_3^{\text{B}}\text{Fe}(\text{NNSiMe}_3)$	1.0	0.3
$[\text{ArP}_3^{\text{B}}\text{Fe}(\text{NNH}_2)][\text{BAR}^{\text{F}}_{24}]$	1.0	0.3

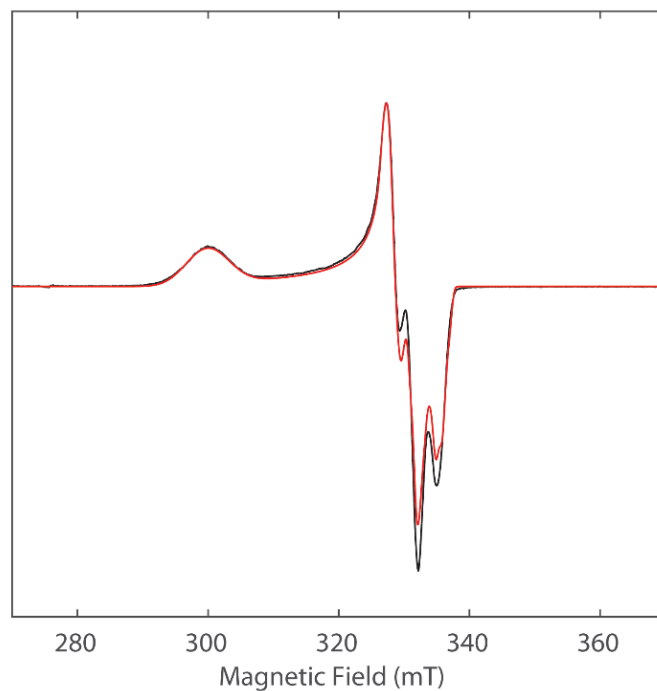


**Figure S13:** CW X-band EPR spectrum of  $^{51}\text{P}_3^{35}\text{Fe}(\text{NNSiMe}_3)$  (black) with simulation (red) using parameters in Table 3 of the main text and broadening parameters  $\text{HStrain} = [170 \ 10 \ 10]$  MHz and  $\text{gStrain} = [0.038 \ 0.002 \ 0.002]$ . Acquisition parameters: temperature = 77 K; MW frequency = 9.44 GHz; MW power = 6.44 mW; modulation amplitude = 0.1 mT; conversion time = 5.12 ms.

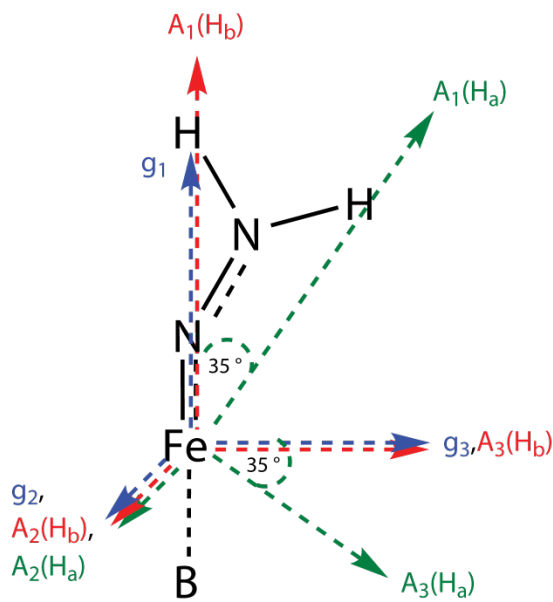


**Figure S14.** Depiction of the Relative Orientation of the Hyperfine Tensor with respect to the molecular frame and g tensor for  $[\text{ArP}_3\text{BFe}(\text{NNH}_2)][\text{BAr}^{\text{F}}_{24}]$ . Phosphine ligands have been omitted for sake of clarity.

**Assays for  $\text{NH}_3$  production:**  $\text{NH}_3$  production was tested under the conditions described according to procedures outlined previously by our group.<sup>1,11</sup>

**Table S3:**  $\text{NH}_3$  Production Under Various Conditions

Precatalyst	Reductant (equiv.)	Acid (equiv.)	Yield (equiv./Fe)
$[(\text{ArP}_3\text{B})\text{Fe}(\text{N}_2)][\text{Na}(12\text{-C-4})_2]^{\text{a}}$	$\text{KC}_8$ (56)	$\text{HBArF}_{24} \cdot 2\text{Et}_2\text{O}$ (46)	.095
$[(\text{ArP}_3\text{B})\text{Fe}(\text{N}_2)][\text{Na}(12\text{-C-4})_2]^{\text{b}}$	$\text{CoCp}^*_2$ (53)	$[\text{H}_2\text{NPh}_2][\text{OTf}]$ (108)	0.0
$[(\text{ArP}_3\text{B})\text{Fe}(\text{N}_2)][\text{Na}(12\text{-C-4})_2]^{\text{c}}$	None	$\text{HBArF}_{24} \cdot 2\text{Et}_2\text{O}$ (2)	0.22
$[(\text{ArP}_3\text{B})\text{Fe}(\text{N}_2)][\text{Na}(12\text{-C-4})_2]^{\text{c}}$	None	$\text{HBArF}_{24} \cdot 2\text{Et}_2\text{O}$ (5)	0.25

<sup>a</sup> Precatalyst, acid, reductant and  $\text{Et}_2\text{O}$  were sealed in a Schlenk tube at 77 K and then warmed to  $-78^\circ\text{C}$  and stirred for 45 minutes followed by stirring for 30 minutes while warming room temperature prior to  $\text{NH}_3$  quantification workup. <sup>b</sup> Precatalyst, acid, reductant and  $\text{Et}_2\text{O}$  were sealed in a Schlenk tube at 77 K and then warmed to  $-78^\circ\text{C}$  and stirred for 6 hours followed by stirring for 30 minutes while warming to room temperature prior to  $\text{NH}_3$  quantification workup. <sup>c</sup> Precatalyst, acid, and  $\text{Et}_2\text{O}$  were sealed in a Schlenk tube at 77 K and then warmed to  $-78^\circ\text{C}$  and stirred for 15 minutes followed by stirring for 30 minutes while warming to room temperature prior to  $\text{NH}_3$  quantification workup.

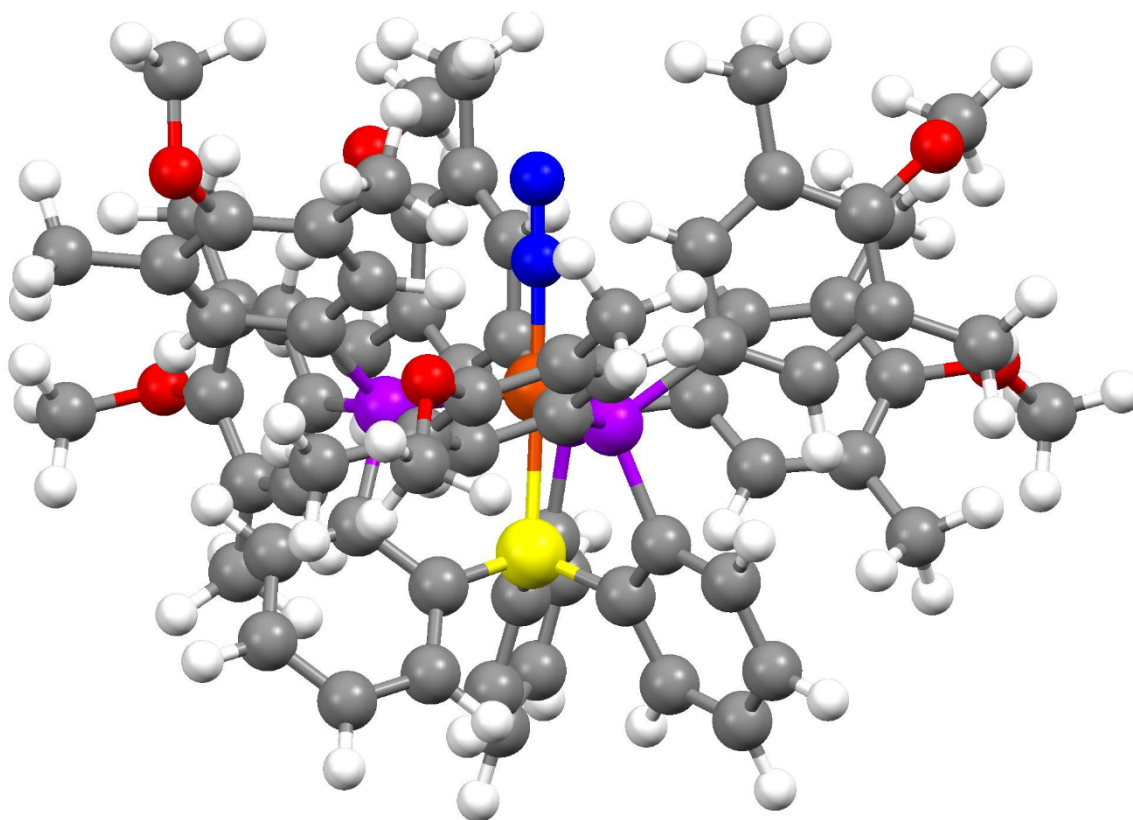


**Figure S15:** DFT optimized structure of a truncated version of  $[\text{ArP}_3\text{BFe}(\text{N}_2)]^-$  (TPSS, def2-TZVP on Fe, def2-SVP on all other atoms) (Isopropyl groups on arene rings replaced with methyl groups). (Fe shown in orange, P shown in purple, B shown in yellow, O shown in red, H shown in white, C shown in gray).

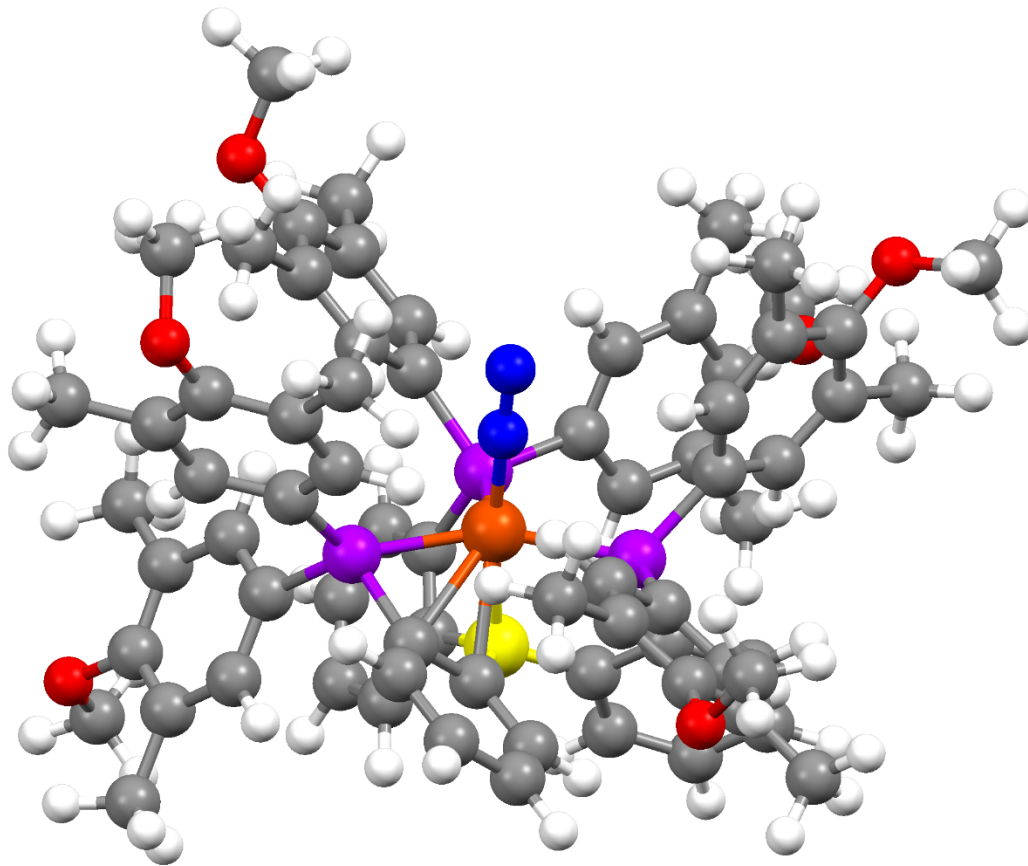


**Figure S16:** DFT optimized structure of a truncated version of  $\text{ArP}_3\text{BFe}(\text{N}_2)$  (TPSS, def2-TZVP on Fe, def2-SVP on all other atoms) (Isopropyl groups on arene rings replaced with methyl groups). (Fe shown in orange, P shown in purple, B shown in yellow, O shown in red, H shown in white, C shown in gray).

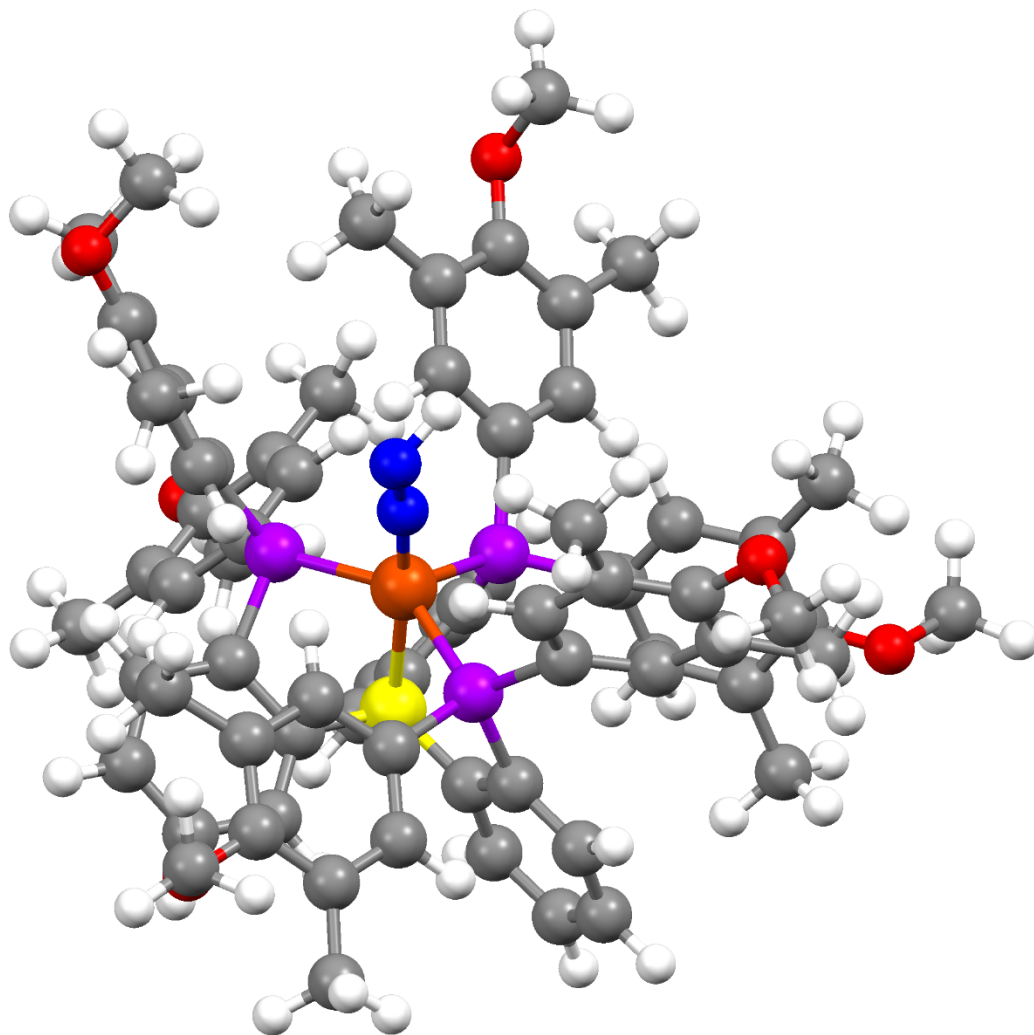


**Figure S17:** DFT optimized structure of a truncated version of  $^{\text{Ar}}\text{P}_3\text{BFe}(\text{NNH})$  (TPSS, def2-TZVP on Fe, def2-SVP on all other atoms) (Isopropyl groups on arene rings replaced with methyl groups). Fe shown in orange, P shown in purple, B shown in yellow, O shown in red, H shown in white, C shown in gray.

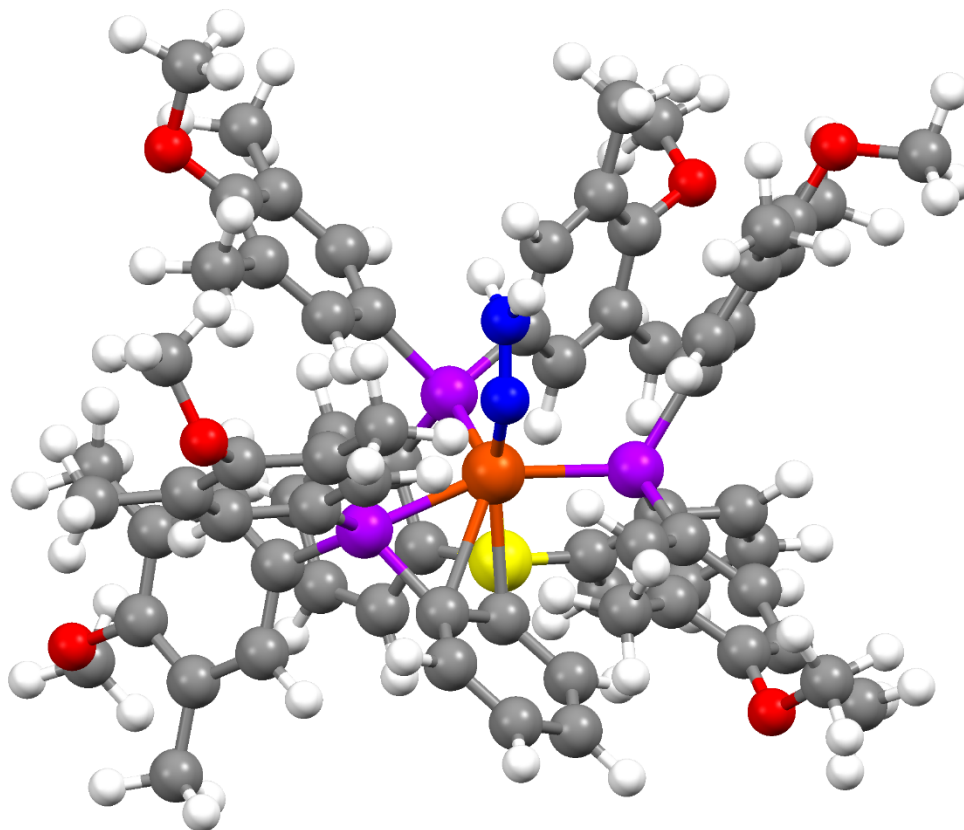


**Figure S18:** DFT optimized structure of a truncated version of  $[\text{ArP}_3\text{BFe}(\text{NNH}_2)]^+$  (TPSS, def2-TZVP on Fe, def2-SVP on all other atoms) (Isopropyl groups on arene rings replaced with methyl groups). Fe shown in orange, P shown in purple, B shown in yellow, O shown in red, H shown in white, C shown in gray.

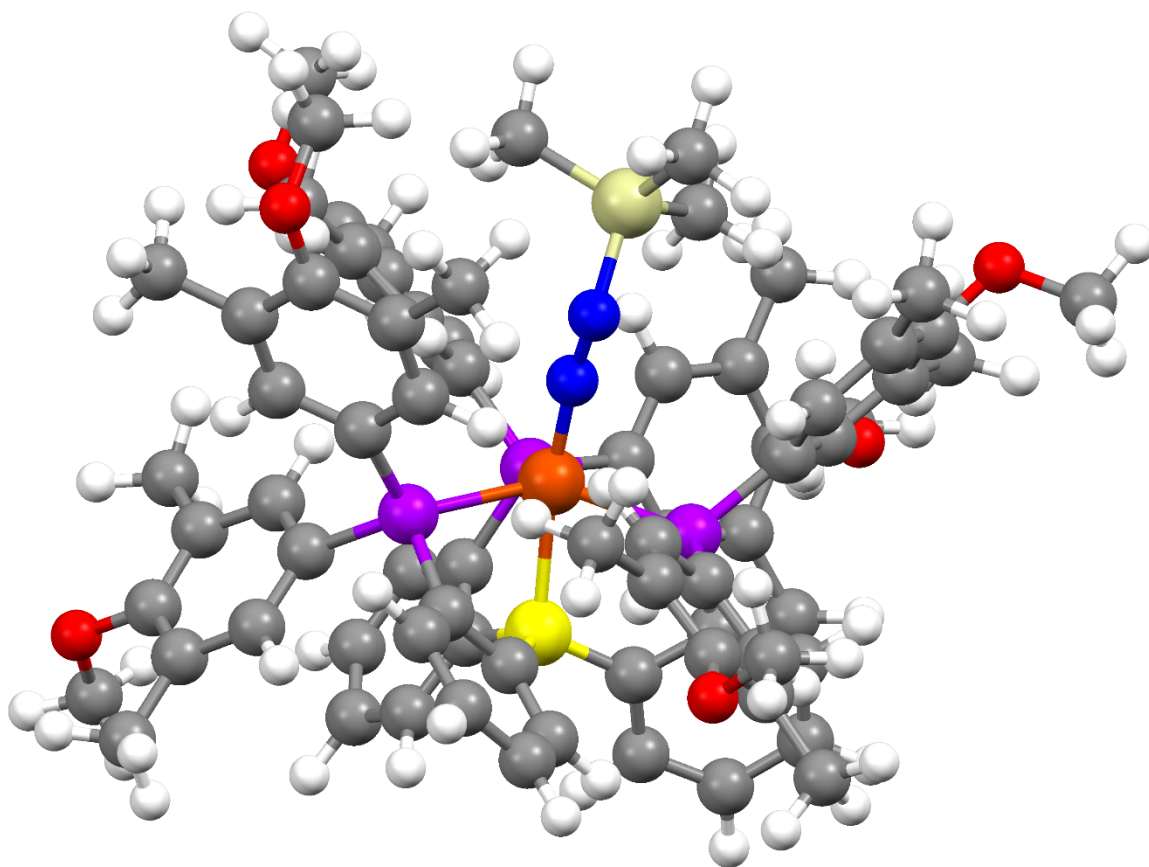


**Figure S19:** DFT optimized structure of a truncated version of  $\text{Ar}_3\text{BFeNNSiMe}_3$  (TPSS, def2-TZVP on Fe, def2-SVP on all other atoms) (Isopropyl groups on arene rings replaced with methyl groups). Fe shown in orange, P shown in purple, B shown in yellow, O shown in red, H shown in white, C shown in gray, Si shown in tan.

**Table S4:** Comparison of Simulated and DFT Calculated EPR Parameters (A values and  $e^2qQ/h$  reported in MHz) calculated using the TPSS functional and CP(PPP) for Fe, IGLO-III for P, Si, B, N, and N-H protons, def2-SV(P) for all other atoms.\*

$[\text{ArP}_3\text{BFe}(\text{N}_2)]^-$	$A_{\text{Sim}}$	$A_{\text{DFT}}$	$e^2qQ/h$	$e^2qQ/h(\text{dft})$	$\eta$	$\eta_{\text{DFT}}$
P <sub>(1)</sub>	(41, 20, 18)	(-56.5, -39.5, -67.1)	N/A	N/A	N/A	N/A
P <sub>(2)</sub>	(63, 48, 42)	(-69.8, -45.1, -78.7)	N/A	N/A	N/A	N/A
P <sub>(3)</sub>	(123, 110, 110)	(97.9, 110.4, 96.4)	N/A	N/A	N/A	N/A
N <sub><math>\alpha</math></sub>	(-1.4, -3.2, 0.7)	(-2.2, -3.4, 0.1)	3.4	-3.2	0.1	0.01
N <sub><math>\beta</math></sub>	N/A	(1.0, -4.7, 3.0)	N/A	-2.5	N/A	0.17
<sup>11</sup> B	(15.2, 15.3, 15.3)	(-19.6, -19.2, -23.3)	0.3	0.73	0.1	0.12
$\text{ArP}_3\text{BFe}(\text{NNH})$						
P <sub>(1)</sub>	(22, 17, 17)	(-9.1, -2.4, -12.5)	N/A	N/A	N/A	N/A
P <sub>(2)</sub>	(22, 17, 17)	(16.2, 22.0, 31.0)	N/A	N/A	N/A	N/A
P <sub>(3)</sub>	(85, 65, 72)	(-63.8, -42.7, -50.9)	N/A	N/A	N/A	N/A
N <sub><math>\alpha</math></sub>	(-2.5, -7.1, 1.8)	(2.3, -1.5, 13.0)	2.0	2.79	0.6	0.25
N <sub><math>\beta</math></sub>	(-2.9, -1.8, 0.7)	(2.8, -2.8, 6.1)	1.8	2.47	0.6	0.99
<sup>11</sup> B	(12, 11.3, 10.5)	(-2.0, -8.3, -7.0)	1.0	1.78	0.3	0.13
H	(19.3, 18.3, 12)	(44.7, 37.7, 37.1)	0.25	0.23	0.1	0.05
$\text{ArP}_3\text{BFe}(\text{NNSiMe}_3)$						
P <sub>(1)</sub>	(25, 16, 26)	(-16.5, -5.1, -22.5)	N/A	N/A	N/A	N/A
P <sub>(2)</sub>	(36, 26, 26)	(-30.4, -55.1, -41.5)	N/A	N/A	N/A	N/A
P <sub>(3)</sub>	(111, 90, 92)	(87.8, 91.5, 112.5)	N/A	N/A	N/A	N/A
N <sub><math>\alpha</math></sub>	(-5.5, -7.6, -1.6)	(-1.2, -6.3, 1.9)	2.0	-1.76	0.6	0.94
N <sub><math>\beta</math></sub>	(-4.0, -4.5, -1.8)	(-8.2, -1.2, 0.0)	1.8	-1.61	0.6	0.99
<sup>11</sup> B	(12.5, 12.7, 13.5)	(-10.6, -11.0, -9.2)	1.0	1.62	0.3	0.16
$[\text{ArP}_3\text{BFe}(\text{NNH}_2)]^+$						
P <sub>(1)</sub>	(40, 16, 23)	(-15.7, -22.8, -10.7)	N/A	N/A	N/A	N/A
P <sub>(2)</sub>	(46, 47, 47)	(-43.3, -45.0, -67.3)	N/A	N/A	N/A	N/A
P <sub>(3)</sub>	(64, 78, 65)	(-54.2, -53.2, -69.2)	N/A	N/A	N/A	N/A
N <sub><math>\alpha</math></sub>	(-0.9, -7.1, 0.1)	(-7.8, 24.4, -0.8)	1.7	-6.99	0.7	0.57
N <sub><math>\beta</math></sub>	XX	(-7.1, -1.7, -0.2)	XX	-3.51	XX	0.33
<sup>11</sup> B	(9.5, 7.5, 6.1)	(-2.4, 10.5, -4.8)	1.0	2.44	0.3	0.14
H <sub>a</sub>	(16, 21, 27)	(48.2, 46.0, 56.1)	0.25	0.24	0.1	0.16
H <sub>b</sub>	(10, 13.5, 12.7)	(18.0, 17.0, 24.7)	0.25	0.23	0.1	0.17

\*note:  $e^2qQ/h$  and  $\eta$  values that have been associated with H ( $\text{ArP}_3\text{BFe}(\text{NNH})$ ) or H<sub>a</sub>/H<sub>b</sub> ( $[\text{ArP}_3\text{BFe}(\text{NNH}_2)]^+$ ) only apply to <sup>2</sup>H isotopologues as <sup>1</sup>H is not a quadrupolar nucleus. The A values listed above are for hyperfine coupling to <sup>1</sup>H. The A values for <sup>2</sup>H can be accordingly calculated by multiplication of the tabulated A value by the appropriate ratio between the gyromagnetic ratios <sup>2</sup>H/<sup>1</sup>H $\gamma = 0.154$ .

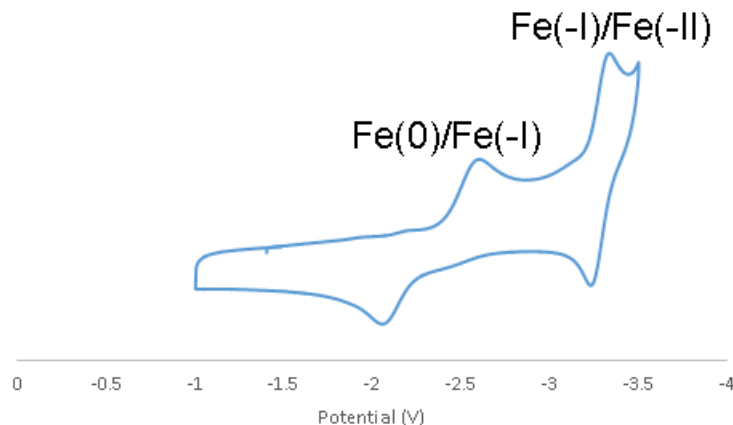


**Figure S20:** Cyclic Voltammogram of  $^{Ar}P_3^BFe(N_2)$  (THF, 0.1 M [TBA][PF<sub>6</sub>]).

### References:

- <sup>1</sup> Del Castillo, T. J.; Thompson, N. B.; Peters, J. C. A Synthetic Single-Site Fe Nitrogenase: High Turnover, Freeze-Quench <sup>57</sup>Fe Mössbauer Data, and a Hydride Resting State. *J. Am. Chem. Soc.* **2016**, *138*, 5341.
- <sup>2</sup> Provencher, L.; Wynn, H.; Jones, J. B.; Krawczyk, A. R. Enzymes in Organic Synthesis 51. Probing the Dimensions of the Large Hydrophobic Pocket of the Active Site of Pig Liver Esterase. *Tetrahedron-Asymmetr.* **1993**, *4*, 2025.
- <sup>3</sup> Weitz, I. S.; Rabinovitz, M. The Application of C<sub>8</sub>K for Organic Synthesis: Reduction of Substituted Naphthalenes. *J. Chem. Soc., Perkin Trans. 1* **1993**, 117.
- <sup>4</sup> Robbins, J. L.; Edelstein, N.; Spencer, B.; Smart, J. C. Syntheses and Electronic Structures of Decamethylmetallocenes. *J. Am. Chem. Soc.* **1982**, *104*, 1882.
- <sup>5</sup> Vicente, J.; Chicote, M.-T.; Guerrero, R.; Jones, P. G. Synthesis of Complexes [Au(PPh<sub>3</sub>)L]<sup>+</sup> (L = primary, secondary or tertiary amine). Crystal Structure of [Au(PPh<sub>3</sub>)(NMe<sub>3</sub>)] [ClO<sub>4</sub>] · CH<sub>2</sub>Cl<sub>2</sub>. *J. Chem. Soc., Dalton Trans.* **1995**, 1251.
- <sup>6</sup> Xu, Y.; Alcock, N. W.; Clarkson, G. J.; Docherty, G.; Woodward, G.; Wills, M. Asymmetric Hydrogenation of Ketones Using a Ruthenium(II) Catalyst Containing BINOL-Derived Monodonor Phosphorus-Donor Ligands. *Org. Lett.* **2004**, *6*, 4105.
- <sup>7</sup> Stoll, S.; Schweiger, A. EasySpin, a Comprehensive Software Package for Spectral Simulation and Analysis in EPR. *J. Magn. Reson.* **2006**, *178*, 42.
- <sup>8</sup> Sheldrick, G. M. Crystal Structure Refinement with SHEL. *Acta Crystallogr. C.* **2014**, *71*, 3.
- <sup>9</sup> Grimme, S.; Antony, J.; Ehrlich, S.; Krieg, H. A Consistent and Accurate *ab initio* Parametrization of Density Functional Dispersion Correction (DFT-D) for the 94 Elements H-Pu. *J. Chem. Phys.* **2010**, *132*, 154104.
- <sup>10</sup> Thompson, N. B.; Oyala, P. H.; Dong, H. T.; Chalkley, M. J.; Zhao, J.; Alp, E. E.; Hu, M.; Lehnert, N.; Peters, J. C. Electronic Structures of an [Fe(NNR<sub>2</sub>)]<sup>+0/-</sup> Redox Series: Ligand Non-Innocence and Implications for Catalytic Nitrogen Fixation. *Inorg. Chem.* **2019**, *58*, 3535.
- <sup>11</sup> Chalkley, M.; Del Castillo, T.; Matson, B.; Roddy, J.; Peters, J. C. Catalytic N<sub>2</sub>-to-NH<sub>3</sub> Conversion by Fe at Lower Driving Force: A Proposed Role for Metallocene-Mediated PCET. *ACS Central Science*, **2017**, *3*, 217.